Article

A Novel Time-Varying P-III Distribution Curve Fitting Model to Estimate Design Floods in Three Gorges Reservoir Operation Period

Yuzuo Xie [1], Shenglian Guo [1,*], Sirui Zhong [1], Xiaoya Wang [1], Jing Tian [2] and Zhiming Liang [3]

[1] State Key Laboratory of Water Resources Engineering and Management, Wuhan University, Wuhan 430072, China; yuzuoxie@whu.edu.cn (Y.X.); zhongsr@whu.edu.cn (S.Z.); 2023202060014@whu.edu.cn (X.W.)
[2] Changjiang Institute of Survey, Planning, Design and Research, Wuhan 430010, China; jingtian@whu.edu.cn
[3] China Yangtze Power Cooperation Ltd., Wuhan 430010, China; liang_zhiming@ctg.com.cn
[*] Correspondence: slguo@whu.edu.cn

Highlights:

What are the main findings?

- Non-stationary design flood estimation considering historical information
- Propose a novel time-varying P-III distribution curve fitting (Tv-P3/CF) model

What is the implication of the main finding?

- Comparative study of reservoir indices and parameter estimation methods helps identify the most effective methods for estimating design floods in varying hydrological contexts.
- Analyze design flood estimation results in Three Gorges Reservoir operation period for reservoir operation

Abstract: Design floods are traditionally estimated based on the at-site annual maximum flood series, including historical information of hydraulic structures. Nevertheless, the construction and operation of upstream reservoirs undermine the assumption of stationarity in the downstream flood data series. This paper investigates non-stationary design flood estimation considering historical information from the Three Gorges Reservoir (TGR) in the Yangtze River. Based on the property that the distribution function of a continuous random variable increases monotonically, we proposed a novel time-varying P-III distribution coupled with the curve fitting method (referred to as the Tv-P3/CF model) to estimate design floods in the TGR operation period, and we comparatively studied the reservoir indices and parameter estimation methods. The results indicate that: (1) The modified reservoir index used as a covariate can effectively capture the non-stationary characteristics of the flood series; (2) The Tv-P3/CF model emphasizes the fitness of historical information, yielding superior results compared to time-varying P-III distribution estimated by the maximum likelihood method; (3) Compared to the original design values, the 1000-year design peak discharge Q_{m} and 3-day and 7-day flood volumes in the TGR operation period are reduced by approximately 20%, while the 15-day and 30-day flood volumes are reduced by about 16%; (4) The flood-limited water level of the TGR can be raised from 145 m to 154 m, which can annually generate 0.32 billion kW h more hydropower (or increase by 6.8%) during flood season without increasing flood prevention risks.

Keywords: cascade reservoirs; non-stationary; time-varying moment; reservoir index; P-III distribution; curve fitting method; maximum likelihood method; Three Gorges Reservoir

1. Introduction

Traditional design floods for hydraulic structures such as reservoirs are based on the at-site annual maximum flood data series being stationary hypothesis, and historical flood events and observed flow discharge data series are used for flood frequency analysis [1].

According to *Specification for Calculating Design Flood of Water Resources and Hydropower Projects* in China [2], Pearson type III (P-III or P3) distribution coupled with the curve fitting method (referred to as the P3/CF model) is recommended to estimate the design flood for a given design frequency. The theoretical frequency curve derived using the P3/CF model, based on the criterion of minimizing the sum of squared deviations between the empirical and model-based frequency points, is plotted on the Hessian probability graph [3]. This plot effectively demonstrates the fit of the annual maximum flood data series, with particular emphasis on the accurate representation of historical flood events. The flood hydrograph of typical year is selected and used to derive the design flood hydrograph using the peak and volume amplitude method [3,4]. Then, the design flood hydrograph is used to determine the reservoir flood prevention storage and characteristic water levels through reservoir flood routing, of which the flood-limited water level (FLWL) is a key parameter to balance flood control risk and comprehensive reservoir benefits [5,6]. This type of design flood is mainly used to determine spillway dimensions and dam height and is referred to as the "design flood in reservoir construction period" [7,8].

In recent decades, climate change and human activities have altered the hydrological regime of rivers [9–13]. As a result, the observed hydrological data series may no longer meet the stationary assumption requirements for the traditional P3/CF model, which means that the statistical properties (such as mean, variance, and skewness) of the annual maximum flood data series have changed [14,15]. Several studies have shown that, among all factors, including global climate change and intensified human activities, the construction and operation of reservoirs is the most significant factor affecting the statistical characteristics of the flow data series [16–20]. Therefore, considering the regulation effects of upstream reservoirs and updating the FLWLs based on the "design flood in reservoir operation period" [8] have significant theoretical and practical value for high-efficient utilization of flood water resources.

Two approaches, the flood regional composition (FRC) method [8,21,22] and non-stationary flood frequency analysis method [23,24], have been used to consider the impacts of upstream reservoirs on downstream design floods. The FRC method relies on a simplified event-based scheme to represent the flood generation mechanisms at the investigated reservoir within the river network and to account for the human-defined operation rules of the reservoirs [8]. The restored natural flood data series used in the FRC method is stationary, while the non-stationarities of reservoir operation are explicitly addressed by the reservoir operation rules. However, hydrologic- or hydraulic-based model simulations generally require a substantial amount of data, which is not always available in practice. Furthermore, the high computational costs associated with these simulations can impede their application on large basins [25,26].

On the other hand, non-stationary flood frequency analysis methods in a changing environment can be classified into three categories. The first one involves the backward or forward reconstruction method [27,28], which employs specific correction measures to eliminate the effects of non-stationarities in the hydrological series caused by cascade reservoirs, thereby the reconstructed stationary series is then used for flood frequency analysis based on the stationary assumption. However, the causes of non-stationarity are very complex. Current methods struggle to fully eliminate the non-stationary factors and restore a stationary series. The second option is to mix multiple distinct distribution functions to account for the heterogeneous nature of the flow data series [29,30]. Nevertheless, this approach is not appropriate for basins with relatively homogeneous flood sources, which represent a special case characterized by a single flood population. An example of such a basin is the Yangtze River, where extreme floods are predominantly driven by heavy storm rainfall [31]. The third category is the time-varying moment method, which embeds certain covariates (time variables and physical predictors that have a causal relationship with the hydrological sequence) to explain the variation in the probability distribution parameters for describing the non-stationary characteristics [32–34]. Rigby and Stasinopoulos (2005) and Stasinopoulos and Rigby (2007) introduced the Generalized Additive Models for Lo-

cation, Scale, and Shape (GAMLSS) model, an efficient tool that enhances the clarity and intuitiveness of time-varying parameter models [35,36]. This development has significantly advanced the field of non-stationary flood frequency analysis in recent years [15,20,37–39], which generally necessitates simplified indices that facilitate a low-cost, implicit quantification of reservoir impact, focusing on a limited number of system characteristics based on the observed behavior. One such index is the reservoir index [40,41], which evaluates the reservoir impact in proportion to the ratio of the total reservoir capacity to the annual mean runoff at the catchment control section.

The GAMLSS model typically employs the maximum likelihood method to estimate time-varying parameter models [42–45]. However, the validity of parameter estimation methods for P-III distribution based on the likelihood function, such as the maximum likelihood and Bayesian methods, is restricted to samples with absolute skewness not greater than two [46]. Furthermore, during the initial design stage of reservoirs based on the stationary assumption, design flood estimation thoroughly incorporates historical flood events, including the magnitude and rank of historical information. The maximum likelihood method, however, accounts for the historical information by assuming that the observed series shares the same order moments as the series from the entire investigation period, excluding extraordinary floods, which potentially increases the uncertainty in design flood estimates [47–49].

The aim of this study is to investigate non-stationary design flood estimation considering historical information in the reservoir operation period and propose a novel time-varying P-III distribution coupled with the curve fitting method (referred to as the Tv-P3/CF model). This approach uniquely emphasizes the integration of time-varying P-III distribution with the curve fitting method, thereby filling a critical gap in the application of the existing maximum likelihood method in non-stationary flood frequency analysis. Furthermore, the consideration of historical flood information can enhance the accuracy of design flood estimates. Moreover, a comparative analysis of various reservoir indices and parameter estimation techniques are conducted to evaluate the model performance. The present paper is structured as follows. Section 2 describes the methodology used in this study. In Section 3, the study area and the material are briefly introduced. Section 4 presents the Three Gorges Reservoir (TGR) on the Yangtze River in China, the world's largest reservoir, selected as a case study. The last two sections are dedicated to the discussion and conclusion of this study, respectively.

2. Methodology

Figure 1 shows the flowchart of non-stationary design flood estimation in the reservoir operation period considering historical information, which comprises four main modules. The first module conducts a preliminary analysis of non-stationarity in the annual maximum flood series by trend analysis and change point detection. The second module constructs the time-varying parameters of P-III distribution with covariates based on the generalized linear additive model and uses the maximum likelihood method to estimate the parameters. In the third module, the Tv-P3/CF model is proposed to estimate design floods in the reservoir operation period. The fourth module derives the design flood hydrograph and analyzes benefits and risks of the TGR.

2.1. Preliminary Analysis of Non-Stationarity Annual Maximum Flood Data Series

Non-stationarity is the opposite of stationarity, meaning that a non-stationary hydrological series can be understood as one that contains trends, discontinuities, or periodicities. Considering that periodicity typically occurs within a year rather than inter-annually, the preliminary diagnosis of non-stationarity in the annual maximum flood series generally does not include periodicity [20]. This module preliminary analyzes the non-stationarity in the annual maximum flood data series using the Mann–Kendall trend test [50–52] and Pettitt's test [53] for change point detection.
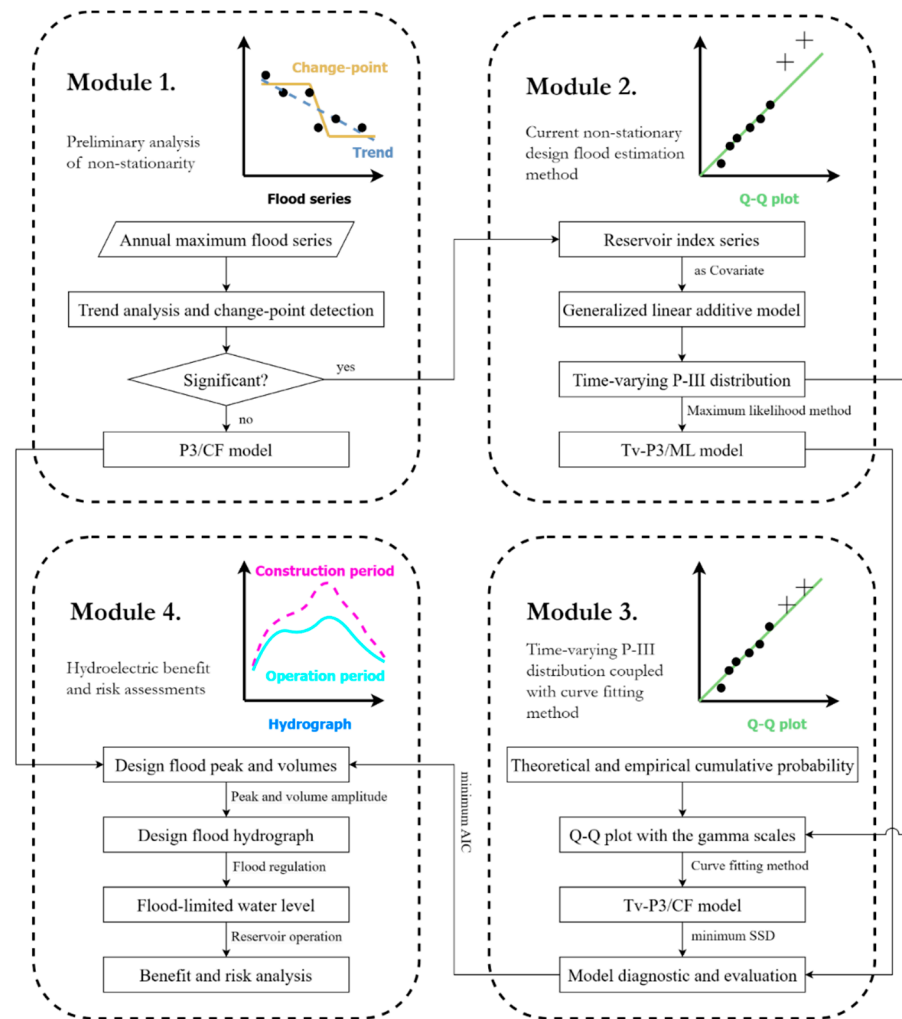
Figure 1. Flowchart of non-stationary design flood estimation in the reservoir operation period considering historical information.

2.1.1. Mann–Kendall Trend Test

For the time series x_1, x_2, ..., x_n (n is the sample number), the Mann–Kendall test is based on testing the S_k statistic, defined as follows:

$$S_k = \sum_{i=1}^{k} \sum_{j=1}^{i} \gamma_{ij} \qquad (k = 1, 2, 3, \cdots, n) \quad \& \quad \gamma_{ij} = \begin{cases} 1 & x_i > x_j \\ 0 & x_i < x_j \end{cases} \tag{1}$$

Assuming that the samples are independent and after standardizing S_k, the statistic UF_k of the Mann–Kendall test is calculated as follows:

$$UF_k = \frac{S_k - E(S_k)}{\sqrt{Var(S_k)}} \tag{2}$$

where $E(S_k)$ and $Var(S_k)$ are the mean and variance of S_k, respectively.

Applying the above steps to the inverse sequence of the time series, the inverse sequence x_n, x_{n-1}, ..., x_1 is denoted as $x'_1, x'_2, \cdots, x'_n$, then UF_k of the inverse sequence is defined as follows:

$$\begin{cases} UB_k = -UF_{k'} \\ k = n + 1 - k' \end{cases} \qquad k = 1, 2, \cdots n \tag{3}$$

If UF_k is greater than 0, the series has an upward trend; otherwise, the series has a downward trend. Given a significance level α, $UF_k > U_\alpha$ means a significant trend change

in the series. Moreover, if the curves of UF_k and UF_k intersect within the interval of the significance level, then the intersection point is the moment when the mutation begins.

2.1.2. Pettitt's Test for Change Point Detection

Based on the assumption that there is no mutation in the sequence, the moment τ satisfies the following relationships:

$$K_\tau = |U_{\tau,n}| = \max(|U_{t,n}|) \quad \& \quad U_{t,n} = \sum_{i=1}^{t} \sum_{j=t+1}^{n} \text{sgn}(x_j - x_i) \qquad 1 \le t \le n \quad (4)$$

where, x_i and x_j are the variables in the sequence to be examined; n is the length of the sample sequence; and $U_{t,n}$ is the new sequence formed based on the number of times the first sample sequence exceeds the second sample sequence.

Then, τ is the point at which the mutation occurs, and the approximate probability for a two-sided test is calculated according to the following:

$$p = 2 \exp\left(\frac{-6K_\tau^2}{T^2 + T^3}\right) \qquad (5)$$

If the p-value is less equal to 0.05, it means that the detected mutation point is significant.

2.2. Current Stationary Design Flood Estimation Method in China

P-III (P3) distribution, a generalized Gamma distribution, is one of the most popular distributions for fitting annual maximum flood magnitudes [54–56], and it has been recommended by the Ministry of Water Resources, China [2], as the standard distribution for stationary flood frequency analysis in China. Let the stationary annual maximum flood data series X follow a P-III distribution with a density function $f(x)$, as follows:

$$f(x) = \frac{\beta^\alpha}{\Gamma(\alpha)}(x - a_0)^{\alpha-1} \exp[-\beta(x - a_0)]$$
$$a_0 < x < +\infty, 0 < \beta < +\infty, 0 < \alpha < +\infty \qquad (6)$$

where $\Gamma(\bullet)$ is the Gamma function; x is a realization of X; and a_0, β, and α are the location, scale, and shape parameters of the P-III distribution, respectively.

The curve fitting method, recommended by the Ministry of Water Resources in China for parameter estimation of P-III distribution, utilizes the sum of squared deviations (SSD) criterion to minimize the discrepancy between the empirical data and model points [2,57]. As a result, P-III distribution coupled with the curve fitting method (P3/CF model) provides a widely applicable approach for estimating design floods under the stationary assumption.

It should be noted that the magnitude of historical flood events significantly exceeds that of observed floods, with their return periods being much longer than those of observed floods. However, extreme values in observed floods can also reach the magnitude of historical flood events. Therefore, both observed extraordinary floods and historically investigated flood events form an extraordinary non-continuous flood series, which requires special treatment in frequency analysis [58]. The plotting position formula for a non-continuous annual maximum flood data series is expressed as follows [57,59]:

$$\tilde{F}_{Y_t}(y_t) = \begin{cases} P_M = \frac{M}{N+1} & M = 1, 2, \ldots, a \\ P_m = \frac{1}{N+1}\left[a + \frac{N-a+1}{n-l+1}(m-l)\right] & m = l+1,\, l+2,\, \ldots,\, n \end{cases} \qquad (7)$$

where P_M and P_m are the empirical frequency of the Mth extraordinary floods and the mth observed floods, respectively; M represents the flood rank in the extraordinary flood sequence ($M = 1, 2, \ldots, a$; a is the number of extraordinary floods); N denotes the length of the entire investigation period, which covers the historical information and observed floods;

m denotes the flood rank in the observed flood sequence; n is the number of observed floods; and l represents the number of floods identified as extraordinary from the observed floods.

2.3. Non-Stationary Design Flood Estimation Method

In non-stationary flood frequency analysis, time-varying moment models for flood variables are typically constructed using the GAMLSS model [60], with parameters currently estimated by the maximum likelihood method [35].

2.3.1. Reservoir Index as Covariates

There are various indicators proposed to implicitly measure the impact of reservoir regulation on the downstream flow regime and flood data series. For example, Batalla et al. (2004) quantified the reservoir impact using the ratio of the total reservoir capacity upstream of a hydrological station to the station's annual average runoff [61]. López and Francés (2013) introduced the reservoir index (RI) based on the drainage area controlled by the reservoir and its regulation capacity [40]. B. Xiong et al. (2019) developed the reservoir–rainfall coupling coefficient based on multi-day antecedent rainfall inputs [62]. The performance of time-varying parameter models varies with different evaluation indicators, which also affects the results of flood frequency analysis. Due to the difficulty of obtaining rainfall data corresponding to historical information and to account for the spatial distribution of upstream reservoirs, the reservoir index (RI) was chosen in this study to measure the impact of reservoirs on the annual maximum flood series, which is expressed as follows:

$$RI = \sum_{j=1}^{J} \left(\frac{A_j}{A} \right) \cdot \left(\frac{V_{\text{tol},j}}{R} \right) \tag{8}$$

where J is the number of upstream reservoirs at the design section; A_j and A denote the catchment area of each reservoir and the design section (km^2), respectively; $V_{\text{tol},j}$ represents the total capacity of each reservoir (billion m^3); and R is the mean annual runoff at the design section (billion m^3).

In reservoir flood control operation, it is reservoir flood regulation storage rather than its total storage capacity that plays a crucial role in mitigating the flood process [6]. Given that the annual runoff distribution at hydrological stations varies throughout the year, the average annual runoff R might not provide an accurate measure of the flood volume during the flood season. Cui et al. (2023) suggested the flood regulation storage $V_{\text{fr},j}$ and multi-year average runoff during the flood season R_f to substitute $V_{\text{tol},j}$ and R in Equation (9), respectively, resulting in the modified reservoir index (MRI), as follows [63]:

$$MRI = \sum_{j=1}^{J} \left(\frac{A_j}{A} \right) \cdot \left(\frac{V_{\text{fr},j}}{R_f} \right) \tag{9}$$

2.3.2. Time-Varying P-III Distribution Coupled with the Maximum Likelihood Method

1. Time-varying P-III distribution

For the non-stationary annual maximum flood data series, it is assumed that the parameters of the distribution function vary with the covariates. Let flood variable Y_t follow the time-varying P-III distribution with a density function $f_{Y_t}(\bullet)$, as follows:

$$f_{Y_t}(y_t | RI; \Omega) = \frac{\beta_t^{\alpha_t}}{\Gamma(\alpha_t)} (y_t - a_{0t}) \alpha_t - 1 \exp[-\beta_t(y_t - a_{0t})]$$
$$a_{0t} < y_t < +\infty, \ 0 < \beta_t < +\infty, \ 0 < \alpha_t < +\infty \tag{10}$$

where y_t is a realization of Y_t; a_{0t}, β_t, and α_t are the location, scale, and shape parameters of the time-varying P-III distribution, respectively; RI denotes the reservoir index, which serves as a covariate in the model; and Ω represents the parameter set of the time-varying P-III distribution.

2. Relationship between covariates and time-varying moments

Presuming that the non-stationarity of the flood series can be explained by the changes in statistical characteristics [54,64], the time-varying moments model can be established by constructing the generalized linear additive formulation of the distribution parameters with respect to a vector of covariates based on the GAMLSS model [35,36]. For time-varying P-III distribution, the following points should be noted:

(1) The shape parameter α_t, which controls the tail behavior of the P-III distribution frequency curve, is highly sensitive to historical flood events [65,66]. It is challenging to determine its causal relationship with the reservoir index when the historical information is limited and the TGR has not been influenced by the regulation of upstream cascade reservoir during those historical flood events. Therefore, the shape parameter of P-III distribution generally remains constant.

(2) The impact of cascade reservoirs on downstream hydrological regimes indicates that reservoir regulation reduces the mean value of the annual maximum flood series [62,66,67]. Given the relationship between the location, scale parameters, and the mean value of the sample, $EY_t = \alpha_t \beta_t^{-1} + a_{0t}$, the mean value is inversely proportional to the location parameter and the reciprocal of the scale parameter. Therefore, the location and scale parameters of P-III distribution can be expressed as functions of the reservoir index [7,60].

(3) To meet sample space constraints and facilitate parameter estimation, the natural logarithm function $\ln(\bullet)$ is chosen as the link function $g_{a_0}(\bullet)$ and $g_\beta(\bullet)$ for a_{0t} and β_t^{-1}, respectively, while the identity function is chosen for the shape parameter α_t [7,66].

In short, let $\Omega = \{\omega_{10}, \omega_{11}, \omega_{20}, \omega_{21}, \omega_{30}\}$, each parameter can be expressed as a function of the (modified) reservoir index via a link function as follows:

$$
\begin{cases}
g_{a_0}(a_{0t}) = \ln(a_{0t}) = \omega_{10} + \omega_{11} \times RI \\
g_\beta\left(\beta_t^{-1}\right) = \ln\left(\beta_t^{-1}\right) = \omega_{20} + \omega_{21} \times RI \\
g_\alpha(\alpha_t) = \alpha = \omega_{30}
\end{cases}
\tag{11}
$$

3. Maximum likelihood estimation method

The maximum likelihood method, which estimates parameters by maximizing the probability distribution's likelihood function, is one of the most commonly used approaches for solving time-varying moment models [35,66]. When incorporating historical flood information, it is generally assumed that the $n - l$ items of the observed flood series correspond to the moments of the same order as the $N - a$ items, excluding an item of extraordinary floods. This assumption equates the geometric mean of the likelihood functions of both the $n - l$ observed series and the $N - a$ series [47,48,58]. Consequently, the maximization of the logarithmic likelihood function, $\ln L$, can be formulated as follows:

$$
\max \ \ln L = \sum_{t=1}^{a} \ln f_{Y_t}(y_t | RI; \Omega) + \frac{N - a}{n - l} \sum_{t=a+1}^{n+a-l} \ln f_{Y_t}(y_t | RI; \Omega)
\tag{12}
$$

Time-varying P-III distribution coupled with the maximum likelihood estimation method is referred as the Tv-P3/ML model in this study. Obviously, when $\alpha_t < 1$, i.e., skewness ≤ 2, the $\ln L$ for a_{0t} is the minimum ordered sample $y_{t(1)} = \min\{y_1, y_2, y_3, \ldots, y_T\}$, then β_t and α_t have no estimates by the maximum likelihood method; the likelihood function goes to infinity as $y_{t(1)} \rightarrow \alpha_t$ [68].

2.3.3. Time-Varying P-III Distribution Coupled with the Curve Fitting Method

This module purposes time-varying P-III distribution coupled with the curve fitting method (Tv-P3/CF model) based on the property that the distribution function of a continuous random variable increases monotonically with the random variable itself.

Under non-stationary conditions, the P3/CF model cannot capture the time-varying parameter characteristics. This study proposes a time-varying P-III distribution coupled with the curve fitting method (Tv-P3/CF model), which acknowledges that despite the

time-varying parameters of P-III distribution not being fixed, the cumulative distribution function $F_{Y_t}(y_t|RI; \Omega)$ continues to increase monotonically with the increase in the annual maximum flood variable y_t. Let $Z_t = F_{Y_t}(Y_t|RI; \Omega)$, then

$$F_{Z_t}(z_t) = \begin{cases} 0 & z_t \leq 0 \\ \begin{aligned} P(F_{Y_t}(Y_t) \leq z_t|RI; \Omega) \quad &= P\left(Y_t \leq F_{Y_t}^{-1}(z_t|RI; \Omega)\right) \\ &= F_{Y_t}\left(F_{Y_t}^{-1}(z_t|RI; \Omega)\Big|RI; \Omega\right) \\ &= z_t \end{aligned} & 0 < z_t < 1 \\ 1 & z_t \geq 1 \end{cases} \quad (13)$$

Thus, $F_{Y_t}(y_t|RI; \Omega)$ follows the standard uniform distribution, i.e., $F_{Y_t}(y_t|RI; \Omega) \sim U(0, 1)$. Based on Equation (13), the process of fitting the empirical frequency points of annual maximum flood samples to the theoretical distribution quantiles of the time-varying P-III distribution is outlined, then the time-varying parameters of P-III distribution are estimated using the curve fitting method.

1. Calculate the theoretical and empirical cumulative probabilities of flood variables

From Equation (13), it is evident that the theoretical cumulative probability of the random variable Z_t is equal to itself, i.e., $F_{Z_t}(z_t) = z_t$. From $Z_t = F_{Y_t}(Y_t|RI; \Omega)$, it follows that $z_t = F_{Y_t}(y_t|RI; \Omega)$ and $F_{Z_t}(z_t) = F_{Y_t}(y_t|RI; \Omega)$. Similarly, the empirical cumulative probability of Z_t can be determined by $\widetilde{F}_{Z_t}(z_t) = \widetilde{z}_t = \widetilde{F}_{Y_t}(y_t)$, according to Equation (13). $\widetilde{F}_{Y_t}(y_t)$ is based on the specific values of flood variates y_t in the non-continuous flood data series, sorted in descending order. The empirical cumulative probabilities of flood variables are calculated by plotting position formulas in Equation (7).

2. Q–Q plot of theoretical and empirical cumulative probabilities

The Q–Q plot (quantile–quantile plot) is a probability plot used to compare two probability distributions by plotting their quantiles against each other [69], which can also be used as a graphical tool for estimating the parameters in a location-scale family of distributions [70]. Then, the Q–Q plot can be utilized to assess the fitness between the empirical frequency and the quantiles of the distribution model, which aids in determining whether the two flood datasets exhibit the same distribution.

To meet the requirements of design flood estimation, which emphatically focuses on observing extreme events based on the historical information in the right tail [2,58], the axes of the Q–Q plot can be adjusted to widen the frequency intervals in the tail region. Given the similarity between the Gamma distribution and the P-III distribution, the inverse cumulative distribution function of the Gamma distribution is used as the coordinate scale. The Q–Q plot is then obtained by plotting the non-continuous sequence points with a length of $n + a - l$, as shown in following equation:

$$\left\{ G^{-1}(\widetilde{z}_t|\alpha, \beta), G^{-1}(z_t|\alpha, \beta); \ t = 1, 2, \ldots, n + a - l \right\} \quad (14)$$

where $G^{-1}(z_t|\alpha, \beta)$ is the inverse cumulative distribution function of the Gamma distribution when the distribution function value equals z_t; and α and β are the shape and scale parameters of the Gamma distribution, respectively. To ensure that the Gamma distribution retains its bell-shaped and right-skewed density curve, which emphasizes the fitting of extraordinary floods, α and β are set to be consistent with those of the P-III distribution frequency curve from the initial design flood results.

3. Estimate the parameters of time-varying P-III distribution using the curve fitting method

In the curve fitting method, it is important to ensure that the curve passes through the center of the points and more emphasis should be placed on the extreme flood points, making the curve as close as possible to the most accurate points [2]. The 1:1 reference line ($y = x$) in the Q–Q plot represents the curve corresponding to the theoretical distribution function. If this reference line passes through the center of the points in the Q–Q plot shown

in Equation (14) (especially the extraordinary flood points), it indicates a good fitness of the distribution function to the empirical frequency. Given the features of linear fitting, this study uses the sum of squares of deviation (SSD) minimum criterion to estimate the parameters of the time-varying P-III distribution [2,57], as follows:

$$\min \ \text{SSD} = \sum_{t=1}^{n+a-l} \left[G^{-1}(z_t | \alpha, \ \beta) - G^{-1}(\widetilde{z}_t | \alpha, \ \beta) \right]^2 \tag{15}$$

The P-III distribution parameters estimated by the P3/CF model in the reservoir construction period served as the initial values for the Tv-P3/CF model in this study.

2.3.4. Model Diagnostics and Evaluation

1. Two-Sample Kolmogorov–Smirnov Test

The Kolmogorov–Smirnov test (K–S test) is a nonparametric statistical test used to assess the equality of one-dimensional probability distributions. It determines whether a sample originates from a given reference probability distribution, known as the one-sample K–S test [71], or whether two samples come from the same distribution, referred to as the two-sample K–S test [29]. This study employs the two-sample K–S test to verify if the distribution function of the theoretical distribution, i.e., Z_t, adheres to the standard uniform distribution. The analysis assumes $Z_t \sim U(0, \ 1)$ as the null hypothesis with a significance level set at 0.05. The null hypothesis is accepted if the *p*-value from the Kolmogorov–Smirnov test exceeds 0.05. Acceptance of the null hypothesis confirms the validity of the theoretical base presented in Equation (15) for parameter estimation of the Tv-P3/CF model.

2. Akaike information criterion

The Akaike information criterion (AIC) is an estimator of prediction error and thus assesses the relative quality of statistical models for a given dataset [72]. A smaller AIC value signifies better fitness of the time-varying P-III distribution than the empirical distribution. Since the P3/CF model measures fitness based on the deviation (or error) between the observed data points and the theoretical distribution curve, it is generally assumed that the deviation follows an independent normal distribution. Consequently, the error-based AIC (referred as AIC_E) can be expressed using least squares model fitting, as follows:

$$\text{AIC}_\text{E} = 2k + (n + a - l) \ln \frac{\sum\limits_{t=1}^{n+a-l} \left(y_t - F_{Y_t}^{-1} \left(\widetilde{F}_{Y_t}(y_t) \mid RI; \Omega \right) \right)^2}{n + a - l} \tag{16}$$

where k represents the number of parameters of the generalized linear additive formulation Ω.

Since the AIC has different versions, the likelihood-based AIC (referred as AIC_L) [35] is also compared in this study.

3. Centile curve

The centile curve plots the centiles for the distributions derived from the time-varying moment model [35,73], which provides a visual assessment of how well the non-continuous flood points align within the estimated percentile ranges of the theoretical time-varying moment model. The calculation formula for the estimated flood variables corresponding to the percentile p is expressed as follows:

$$\hat{y}_t = F_{Y_t}^{-1}(p | RI; \ \Omega) \tag{17}$$

2.4. Hydroelectric Benefit and Risk Assessment

This module mainly derives the design flood hydrograph, analyzes the hydroelectric benefits, and assesses the flood control risks of the TGR. In the reservoir operation period, the design flood hydrograph of the TGR is derived using the peak and volume amplitude method [3,4] based on the design flood results. Then, the FLWL in the operation period

is determined through an iterative calculation approach [74], which ensures that flood prevention standards remain unchanged [75].

2.4.1. Hydroelectric Benefit Analysis

Based on the FLWL derived in the operation period, the reservoir operation model during flood season for the TGR was constructed. Subsequently, the analysis of flood control risk and hydropower benefits was compared against the FLWL in the construction period. The reservoir operation model is presented as follows:

$$\begin{cases} \overline{E} = \sum_{i=1}^{M} \sum_{t=1}^{T} N_i(t) \cdot \Delta t / M \\ N_i(t) = K \cdot Q_i(t) \cdot H_i(t) \end{cases} \tag{18}$$

where $\overline{E}$ is the multi-year average power generation (kW·h) during flood season; $N_i(t)$ denotes the power output of the ith year in period t, MW; Δt is the time step, day; M presents the number of years; K represents hydropower efficiency of the ith reservoir, constant; $Q_i(t)$ denotes discharge release from turbines of the ith reservoir in period t, m^3/s; and $H_i(t)$ is the average hydropower head of the ith reservoir in period t, m.

In addition, a series of physical and operational constraints are imposed on the reservoir operation model in the interest of reservoir management and downstream stakeholders, such as the water balance equation, reservoir water level limits, water level fluctuation rate, reservoir outflow limits, and boundary conditions [76,77], as follows:

$$V_i(t+1) - V_i(t) = (I_i(t) - O_i(t)) \cdot \Delta t - ES_i(t) = 0 \tag{19}$$

$$O^{\min} \leq O_i(t) \leq O^{\max} \tag{20}$$

$$N^{\min} \leq N_i(t) \leq N^{\max} \tag{21}$$

$$Z_i(t) = Z_{\text{FLWL}}, \quad t = 1, \dots, T \& i = 1, \dots, M \tag{22}$$

where $V_i(t)$, $Z_i(t)$, and $I_i(t)$ denote the reservoir storage (m^3), water level (m), and inflow (m^3/s) of the ith year in period t, respectively; $ES_i(t)$ is the sum of evaporation and seepage from the ith year in period t, m^3; $O_i(t)$ presents the discharge (m^3/s) of the ith year in period t, which is between the allowable minimum and maximum discharges, i.e., $O^{\min}$ and $O^{\max}$ (m^3/s); $N^{\min}$ and $N^{\max}$ are the allowable minimum and maximum hydropower outputs, MW, respectively; and Z_{FLWL} denotes the flood-limited water level.

2.4.2. Flood Control Risk Assessment

The TGR's primary flood control responsibility encompasses the downstream Jing River reach and Chenglingji section, which serves as the outlet control station of the Dongting Lake Basin. The designed operation rules of the TGR require that the FLWL is set at 145 m from June to September, reserving 5.65 billion m^3 of flood prevention storage between 145 m and 155 m especially for the Chenglingji section. When the flood in the Dongting Lake Basin is below 15,000 m^3/s and the water level of the Chenglingji station remains under 28.5 m, the available 7 billion m^3 storage of the Dongting Lake Basin is sufficient to manage its own flood waters [78] and does not need to utilize TGR's flood prevention storage. Additionally, the 16.5 billion m^3 of flood prevention storage between 155 m and 175 m in the TGR is allocated solely for the Jing River reach. Therefore, when (1) the inflow into the Dongting Lake Basin is below 15,000 m^3/s and the water level at Chenglingji is under 28.5 m, and (2) TGR's water level remains below 155 m, there is no elevated flood control risk of the TGR.

3. Study Basin and Materials

3.1. Study Basin and Reservoirs

The Yangtze River is the longest river in Asia and the third longest in the world, stretching approximately 6418 km from its source in the Tanggula Mountains of the Tibetan Plateau to its river mouth in the East China Sea. Upstream of the Yichang hydrological station, known as the upper reaches of the Yangtze River, spans 4504 km, encompasses a catchment area of 1 million km^2, and traverses the first and second steps of China's geographical terrain, which is abundant in water and hydro-energy resources. There are over 40,000 reservoirs with various types that have been constructed on the main and tributary streams in the upper Yangtze River, including the Jinsha River, Yalong River, Min River, Jialing River, Wu River, and the Yangtze River main stream. Among these, more than 300 are large reservoirs with a total regulation capacity exceeding 180 billion m^3 and a flood control capacity of approximately 80 billion m^3. Figure 2 shows the topological map and spatial pattern of the major controlling reservoirs in the upper Yangtze River and hydrological stations. Table 1 details the characteristic parameters of the major controlling reservoirs that have been built in the upper Yangtze River Basin.

The TGR is a multipurpose hydro-junction project located at Yichang city, Hubei province. It has a total storage capacity of 39.3 billion m^3, with 22.15 billion m^3 designated for flood prevention. The TGR's flood prevention storage can effectively mitigate flood risks in the downstream Jing River reach and Chenglingji flood control areas, which are historically prone to frequent and devastating flood damages. Additionally, the TGR has a firm output of 4990 MW, a total installed hydropower capacity of 22.5 GW, and generates about 88.2 billion kW·h of hydroelectricity annually.

3.2. Dataset

The Yangtze River Water Resources Commission (YWRC) has conducted extensive investigations of historical flood events in the Yangtze River Basin through both field surveys and literature verification. The information gathered from gauging authority records, historical documents, archives, flood marks, and stone inscriptions accurately indicate the specific locations of recorded high water stages [59]. To ensure that the design of the TGR was both reasonable and reliable, the YWRC and other relevant entities quantitatively extended the record of annual peak discharge at the Yichang station, the dam site gauging hydrologic station of the TGR, back to the early twelfth century. This extension included nine historical flood events that occurred in 1153, 1227, 1560, 1613, 1788, 1796, 1860, and 1870, which are summarized in Table 2 [57,79]. The annual maximum flood series, including peak flood discharge (Q_m), 3-day (W_{3d}), 7-day (W_{7d}), 15-day (W_{15d}), and 30-day (W_{30d}) flood volumes at the Yichang hydrological station for the years 1877 to 1990, along with the eight historical flood events, were used to determine the design flood at the dam site during the design and planning stage of the TGR [79]. Since the construction of the TGR in 2003, inflow data have been consistently recorded. However, the transition of the dam site from a riverine to a lacustrine environment has made direct flow measurements at the dam site unfeasible. This study adopts the approach outlined by Shu et al. (2017), which employed a straightforward linear relationship equation between inflow and dam site floods to estimate the post-2003 annual maximum flood peaks and flood volumes at the dam site [80].

Since observations began at the Yichang hydrological station, three significant Yangtze River floods occurred in 1954, 1998, and 2020, and the latter presented the largest incoming inflow of the TGR since its construction and operation periods. Comparative studies conducted with the reconstructed flood data of the Yangtze River [31,81,82] indicated that the annual maximum 15-day and 30-day flood volumes in 1954 and the annual maximum 30-day flood volume in 1998 exceeded historical flood magnitude levels and were classified as extraordinary floods. By contrast, the flood in 2020 did not surpass historical magnitudes and was therefore treated as an observed flood rather than as an extraordinary flood. Table 2 also provides the annual maximum flood values of the TGR's dam site in 1954, 1998,

and 2020, respectively. In this study, the annual maximum flood data series for the TGR is derived based on the observed flow discharge from 1877 to 2022 and the historical flood events mentioned above in Table 2.
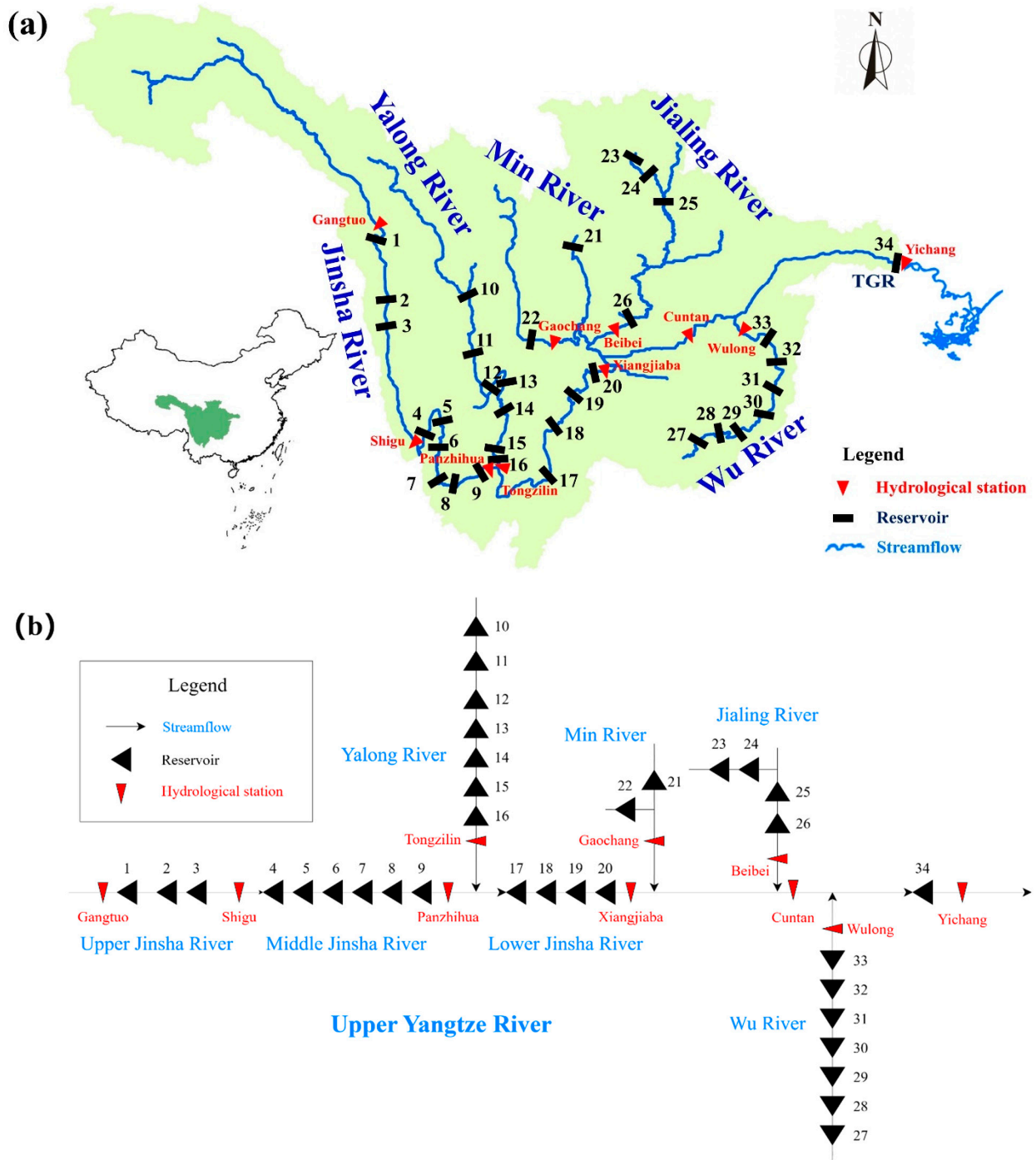

Figure 2. (**a**) Topological map and (**b**) spatial pattern of the major controlling reservoirs in the upper Yangtze River and hydrological stations. (Reservoir numbers are detailed in Table 1).

Table 1. List of the characteristic parameters of the major controlling reservoirs in the Upper Yangtze River.

River Basin	Reservoir Name	Reservoir Number	Catchment Area (10^4 km^2)	Normal Pool Level (m)	Total Storage (Billion m^3)	Regulation Storage (Billion m^3)	Flood Prevention Storage (Billion m^3)	Installed Hydropower capacity (GW)	Operation Year
Upper Jinsha River Basin	Boluo	1	16.05	2989	0.837	0.099	/	0.96	2022
	Batang	2	17.64	2545	0.158	0.026	/	0.74	2022
	Suwalong	3	18.38	2475	0.674	0.084	/	1.20	2021
Middle Jinsha River Basin	Liyuan	4	22.00	1618	0.805	0.173	0.173	2.40	2016
	Ahai	5	23.54	1504	0.885	0.238	0.215	2.00	2014
	Jinanqiao	6	23.74	1418	0.913	0.346	0.158	2.40	2012
	Longkaikou	7	24.00	1298	0.558	0.113	0.126	1.80	2014
	Ludila	8	24.73	1223	1.718	0.376	0.564	2.16	2014
	Guanyinyan	9	25.65	1134	2.25	0.555	0.542	3.00	2016
Yalong River Basin	Lianghekou	10	6.57	2865	10.8	6.56	2.144	3.00	2022
	Yangfanggou	11	8.09	2094	0.512	0.0538	/	1.50	2022
	Jinping-I	12	10.26	1880	7.99	4.911	1.60	3.60	2014
	Jinping-II	13	10.27	1646	0.0192	0.005	/	4.80	2014
	Guandi	14	11.01	1330	0.76	0.123	/	2.40	2013
	Ertan	15	11.64	1200	5.8	3.37	0.90	3.30	1999
	Tongzilin	16	12.76	1015	0.091	0.015	/	0.60	2016
Lower Jinsha River Basin	Wudongde	17	40.61	975	7.408	3.02	2.44	10.20	2021
	Baihetan	18	43.03	825	20.627	10.4	7.5	16.00	2022
	Xiluodu	19	45.44	600	12.67	6.46	4.65	12.60	2014
	Xiangjiaba	20	45.88	380	5.163	0.903	0.903	6.00	2014
Min River Basin	Zipingpu	21	2.27	877	1.112	0.774	0.167	0.76	2006
	Pubugou	22	6.85	850	5.332	3.894	1.1	3.60	2010
Jialing River Basin	Bikou	23	2.60	704	0.217	0.146	0.156	0.30	1997
	Baozhusi	24	2.84	588	2.55	1.34	0.28	0.70	1998
	Tingzikou	25	6.11	458	4.067	1.732	1.44	1.10	2014
	Caojie	26	15.61	203	2.218	0.065	0.199	0.50	2011

Table 1. *Cont.*

River Basin	Reservoir Name	Reservoir Number	Catchment Area (10^4 km²)	Normal Pool Level (m)	Total Storage (Billion m³)	Regulation Storage (Billion m³)	Flood Prevention Storage (Billion m³)	Installed Hydropower capacity (GW)	Operation Year
	Hongjiadu	27	0.99	1140	4.947	3.361	/	0.60	2005
	Dongfeng	28	1.82	970	1.025	0.491	/	0.57	1996
	Wujiangdu	29	2.78	760	2.3	0.928	/	1.25	2003
Wu River Basin	Goupitan	30	4.33	630	6.454	2.902	0.4	3.00	2009
	Silin	31	4.86	440	1.593	0.317	0.184	1.05	2010
	Shatuo	32	5.45	365	0.921	0.287	0.209	1.12	2013
	Pengshui	33	6.90	293	1.465	0.518	0.232	1.75	2009
Upper Yangtze River	TGR	34	100.0	175	39.3	27.894	22.15	22.5	2008

Table 2. List of historical invited and observed floods at TGR dam site.

Hydrological Data Type	Year	Q_m (m^3/s)	W_{3d} (Billion m^3)	W_{7d} (Billion m^3)	W_{15d} (Billion m^3)	W_{30d} (Billion m^3)
Historical information	1870	105,000 (1)	26.50 (1)	53.66 (1)	97.51 (1)	165.0 (1)
	1860	92,500 (2)	23.20 (2)	47.38 (2)	83.57 (5)	145.4 (5)
	1788	86,000 (3)	21.56 (3)	44.19 (3)	78.50 (7)	136.8 (8)
	1153	92,800 (4)	23.27 (4)	47.53 (4)	/	/
	1227	96,300 (5)	24.16 (5)	49.25 (5)	/	/
	1560	93,600 (6)	23.48 (6)	47.92 (6)	/	/
	1796	82,200 (7)	20.60 (7)	42.32 (7)	/	/
	1613	81,000 (8)	20.30 (8)	41.73 (8)	/	/
Observed major floods	1954	66,100	17.01	38.53	78.51 (6)	138.7 (6)
	1998	61,700	15.13	34.78	72.82	138.0 (7)
	2020	65,600	16.70	35.78	62.74	102.7

Note: The data in parentheses indicate the ranks of the extraordinary floods.

4. Result Analysis

4.1. Preliminary Analysis of Non-Stationarity Flood Data Series

At a significance level of 0.05, both the Mann–Kendall trend test and Pettitt's change point test were administered to the annual maximum of the Q_m, W_{3d}, W_{7d}, W_{15d}, and W_{30d} series at the TGR dam site, respectively. The Mann–Kendall trend test yielded statistic values UF_k of −2.71, −2.44, −2.26, −2.58, and −2.61, with corresponding *p*-values of 0.006, 0.014, 0.023, 0.009, and 0.009, respectively, showcasing a prevalent and significant downward trend in the annual maximum flood series. Concurrently, Pettitt's test for detecting change points in the annual maximum series produced statistics U^* of 1720, 1655, 1705, 1787, and 1762, with corresponding *p*-values of 0.007, 0.010, 0.007, 0.004, and 0.005, respectively, highlighting significant change points in 1967. These trends, clearly depicted in Figure 3, emphasized the declining patterns for the annual maximum flood peak Q_m and 15-day flood volume W_{15d}.

4.2. Non-Stationary Flood Frequency Analysis

During flood season, the reservoir flood prevention storage is reserved for flood control purpose. Figure 4 displays the reservoir index (RI, calculated by Equation (8)) and the modified reservoir index (MRI, calculated by Equation (9)) for the key controlling reservoirs in the upper Yangtze River Basin. The chart demonstrates that the construction of major reservoirs in the upper Yangtze River Basin started in the late 1870s and has exerted the strongest influence on the RI and MRI. The large-scale reservoirs constructed after 2014, including Jinping-I, Xiluodu, Xiangjiaba, Lianghekou, and Baihetan, have significantly contributed to the RI and MRI. Overall, the operation of upstream cascade reservoirs has a considerable influence on the downstream annual maximum peak discharge and flood volumes.

For the non-stationary flood frequency analysis of the TGR, the data series included historical flood events and observed floods. It is crucial to recognize that, in the time-varying P-III distribution model, although the annual maximum flood variates and the covariate series are predetermined, the values of parameters ω_{11} and ω_{21} significantly affect the model's functional outcomes. As a result, the rank associated with each flood varies with the values of ω_{11} and ω_{21}. To accurately control the influence of the reservoir index covariate on flood frequency, this study ensured that the number of extraordinary floods and their respective rankings remained unchanged, as detailed in Equation (7) and Table 2, throughout the parameter estimation process for the time-varying P-III distribution.
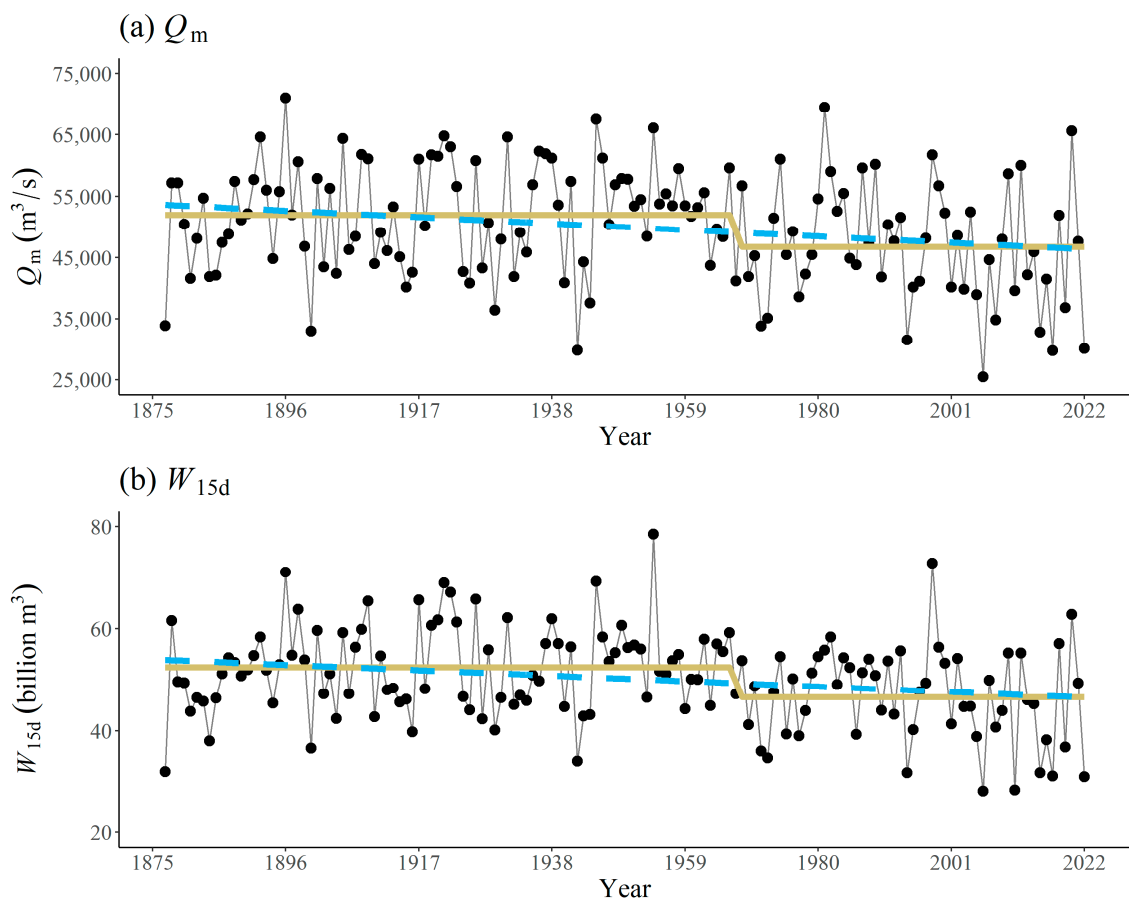
Figure 3. The annual maximum Q_m and W_{15d} with the fitted linear trend lines (dashed lines) and change point detection (solid lines) of the TGR.
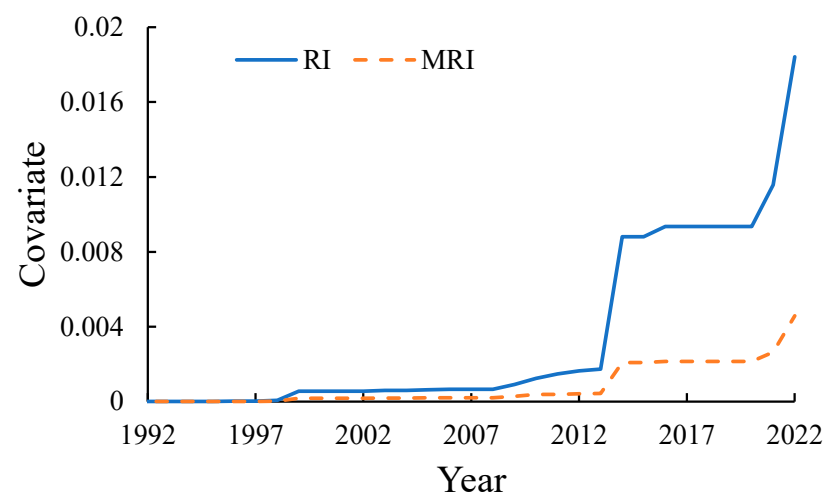

Figure 4. Reservoir index (RI) and the modified reservoir index (MRI) for the key controlling reservoirs in the upper Yangtze River Basin.

A generalized additive model was developed to associate the time-varying P-III distribution with the covariates, including the RI and MRI. The skewness (Cs) from the preliminary design flood results for the TGR were generally below 1.0, which ensured that the maximum likelihood method could be used for parameter estimation of the time-varying P-III distribution. It should be noted that, when performing parameter estimation, no restrictions are imposed on the parameter limits to ensure that the final optimized

parameters do not converge at the boundaries. Tables 3 and 4 present a comparative analysis of parameter estimates and goodness-of-fit metrics between the Tv-P3/ML and Tv-P3/CF models using the RI and MRI as covariates, respectively. The results showed: (a) All the *p*-values of K-S test exceeded 0.05, supporting the null hypothesis that both the empirical frequency distribution of measured flood variates and the time-varying P-III distribution conformed to a uniform distribution across the (0, 1) interval, thus affirming the effectiveness of the Tv-P3/CF model for parameter estimation. (b) The estimates for parameters ω_{11} and ω_{21} from both the Tv-P3/ML and Tv-P3/CF models were negative, indicating that the RI had a reducing effect on the mean values of the flood variates, in line with the relationship between the location, scale parameters, and the overall sample mean. (c) The AIC_E (AIC_L) values for the Tv-P3/CF model were consistently lower (higher) than those of the Tv-P3/ML model across the distribution parameter estimates for the flood peaks Q_m, W_{3d}, W_{7d}, W_{15d}, and W_{30d}, signifying a superior fitness compared to the empirical data in terms of the deviation between observed data points and the theoretical distribution curve. (d) The AIC_E values for the Tv-P3/CF model using the MRI as a covariate were lower than those using RI, indicating that the MRI provided a better fit for the flood series.

Table 3. Estimated parameters and test results of Tv-P3/CF and Tv-P3/ML with RI covariate.

Model	Flood Variates	Parameter					K-S Test	SSD	AIC_E	AIC_L
		ω_{10}	ω_{11}	ω_{20}	ω_{21}	ω_{30}				
Tv-P3/ML	Q_m	6.32	−8.05	7.59	−9.83	25.28	0.32	1.50×10^9	2455.62	−9229.34
	W_{3d}	3.02	−4.60	1.59	−4.32	21.25	0.15	1.75×10^4	684.03	−4040.92
	W_{7d}	2.04	−8.89	2.30	−9.94	26.02	0.37	1.83×10^4	781.87	−4653.52
	W_{15d}	3.42	−4.94	2.87	−5.93	26.85	0.37	2.52×10^4	841.81	−5166.65
	W_{30d}	4.24	−4.57	3.39	−4.84	27.90	0.36	5.15×10^4	1022.02	−5657.35
Tv-P3/CF	Q_m	9.42	−7.06	8.22	−9.57	10.19	0.08	3.47×10^8	2428.29	−9258.79
	W_{3d}	4.26	−14.95	2.59	−14.47	4.22	0.07	1.70×10^3	551.92	−4049.05
	W_{7d}	4.32	−12.15	2.88	−13.43	10.87	0.11	4.20×10^3	710.06	−4662.87
	W_{15d}	5.18	−7.96	3.37	−8.90	11.32	0.35	1.11×10^4	818.09	−5173.46
	W_{30d}	5.50	−7.40	3.72	−7.67	15.90	0.25	2.96×10^4	1011.60	−5662.91

Table 4. Estimated parameters and test results of Tv-P3/CF and Tv-P3/ML with MRI covariate.

Model	Flood Variates	Parameter					K-S Test	SSD	AIC_E	AIC_L
		ω_{10}	ω_{11}	ω_{20}	ω_{21}	ω_{30}				
Tv-P3/ML	Q_m	6.53	−33.34	7.58	−37.80	25.46	0.32	1.56×10^9	2458.69	−9229.25
	W_{3d}	3.24	−24.09	1.84	−29.20	16.02	0.46	6.76×10^3	593.31	−4039.87
	W_{7d}	2.16	−21.83	2.31	−29.72	25.81	0.31	1.87×10^4	786.10	−4653.28
	W_{15d}	3.60	−22.99	2.90	−23.86	25.78	0.44	2.28×10^4	834.19	−5165.66
	W_{30d}	4.31	−17.58	3.44	−19.88	26.60	0.31	4.39×10^4	1012.47	−5657.14
Tv-P3/CF	Q_m	9.91	−41.52	8.36	−47.70	7.10	0.17	3.03×10^8	2398.03	−9258.61
	W_{3d}	4.01	−57.55	2.45	−52.26	6.13	0.08	1.43×10^3	533.93	−4048.75
	W_{7d}	4.31	−56.07	2.87	−56.86	10.92	0.10	4.17×10^3	708.22	−4662.78
	W_{15d}	5.26	−34.18	3.39	−33.95	10.54	0.32	1.09×10^4	817.12	−5173.37
	W_{30d}	5.79	−28.76	3.84	−29.27	12.47	0.28	2.77×10^4	1003.88	−5662.94

It should be noted that the error-based AIC was chosen in this paper for the following reasons: (a) According to the *Specification for Calculating Design Flood of Water Resources and Hydropower Projects* in China, the sum of squared deviations is recommended as the goodness-of-fit measure for design flood estimation. (b) The error-based AIC places a stronger emphasis on historical flood data than the likelihood-based AIC, especially when using the inverse cumulative distribution function of the Gamma distribution as the axes

scale in the Q-Q plot. (c) The likelihood-based AIC lacks universality in practical applications. As indicated in Section 2.3.2, the application of the maximum likelihood method to P-III distribution may result in an unsolvable situation.

To more intuitively demonstrate the goodness-of-fit of the results estimated by the Tv-P3/ML and Tv-P3/CF models with the MRI as the covariate, respectively, Figures 5 and 6 present the Q–Q plots and centile curve graphs based on the annual maximum peak flow Q_m, flood volume W_{7d} and W_{30d}, with the inverse cumulative distribution of the Gamma distribution as the axis scales. Comparative analysis shows: (a) The Q–Q plots reveal that the empirical and frequency quantiles estimated by the Tv-P3/CF model aligned more closely with the 1:1 reference line than those obtained through the Tv-P3/ML model, especially for historical flood events, which suggests that the former more effectively captured the right-tail characteristics of the P-III distribution. (b) The quantile curves indicate that, during the observation period, the flood data series generally fell within the model's quantile range, and the trend in quantile changes was consistent with the observed data trend. This consistency implied that the non-stationary time-varying moment model successfully detected the decreasing trends in the annual maximum Q_m, W_{7d}, and W_{30} at the TGR since the 1990s. Additionally, the 97.5% quantile line derived from the Tv-P3/CF model was higher than that from the Tv-P3/ML model, further indicating its more comprehensive consideration of historical flood events.
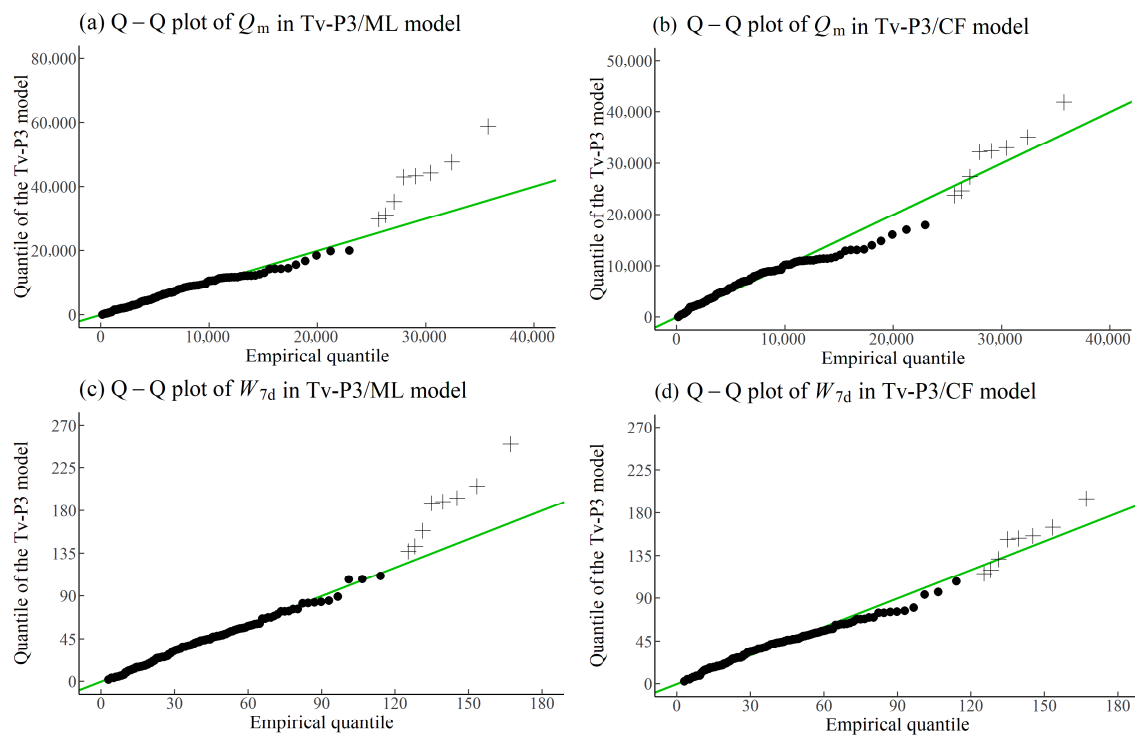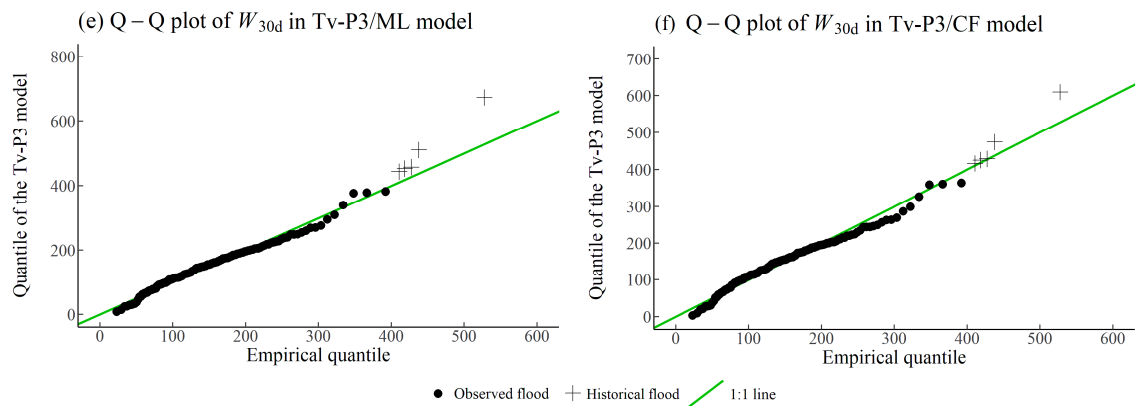

(a) Q − Q plot of Q_m in Tv-P3/ML model

(b) Q − Q plot of Q_m in Tv-P3/CF model

(c) Q − Q plot of W_{7d} in Tv-P3/ML model

(d) Q − Q plot of W_{7d} in Tv-P3/CF model

Figure 5. *Cont.*

(e) Q − Q plot of W_{30d} in Tv-P3/ML model

(f) Q − Q plot of W_{30d} in Tv-P3/CF model

● Observed flood ＋ Historical flood ╱ 1:1 line

Figure 5. Q–Q plots of (**a**) Q_m, (**c**) W_{4d}, and (**e**) W_{30d} in the Tv-P3/ML model and (**b**) Q_m, (**d**) W_{4d}, and (**f**) W_{30d} in the Tv-P3/CF model at the TGR dam site, respectively.
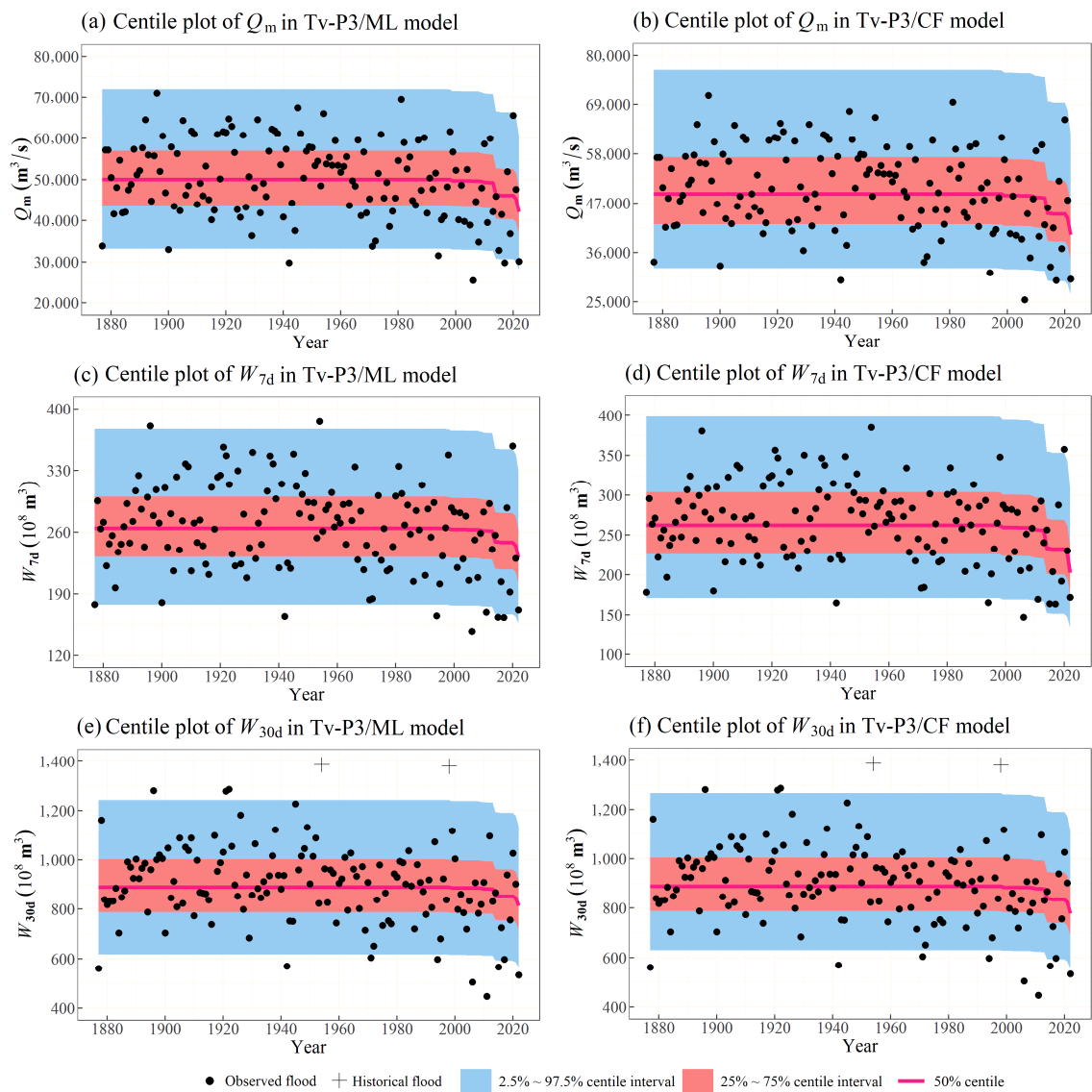
(a) Centile plot of Q_m in Tv-P3/ML model

(b) Centile plot of Q_m in Tv-P3/CF model

(c) Centile plot of W_{7d} in Tv-P3/ML model

(d) Centile plot of W_{7d} in Tv-P3/CF model

(e) Centile plot of W_{30d} in Tv-P3/ML model

(f) Centile plot of W_{30d} in Tv-P3/CF model

● Observed flood ＋ Historical flood ▬ 2.5% ~ 97.5% centile interval ▬ 25% ~ 75% centile interval ▬ 50% centile

Figure 6. Centile plots of (**a**) Q_m, (**c**) W_{4d}, and (**e**) W_{30d} in the Tv-P3/ML model and (**b**) Q_m, (**d**) W_{4d}, and (**f**) W_{30d} in the Tv-P3/CF model at the TGR dam site, respectively.

4.3. Comparative Analysis of Design Floods

The flood data series was restored and extended to 2022, and the design flood was re-checked based on the P3/CF model with the minimum SSD criterion applied during the initial design period. Based on the characteristic parameters of the upstream reservoirs of the TGR, as listed in Table 1, the MRI in 2022 was calculated as 0.0046. Then, using the generalized additive model parameters of the time-varying P-III distribution estimated by Tv-P3/ML and TV-P3/CF models, as shown in Table 4, the estimated design floods are presented in Table 5. The key findings include: (a) The C_v and C_s derived from the Tv-P3/ML model were lower than those from the P3/CF and Tv-P3/CF models, resulting in a flatter frequency curve that did not emphasize the fitting of historical flood events (as shown in Figure 7). Conversely, the Tv-P3/CF model primarily adjusted the mean value of the design flood peak and volumes, with minor changes in C_v and C_s compared to the initial design outcomes. (b) The percentages in Table 4 represent the reduction rate of the design values relative to the P3/CF results. The non-stationary flood frequency analysis, with the MRI as the covariate, showed a reduction in the design floods. Specifically, the design flood peak Q_m and the 3-day and 7-day flood volumes W_{3d} and W_{7d}, were reduced by approximately 20%, while the 15-day and 30-day flood volumes W_{15d} and W_{30d} were reduced by about 16%.
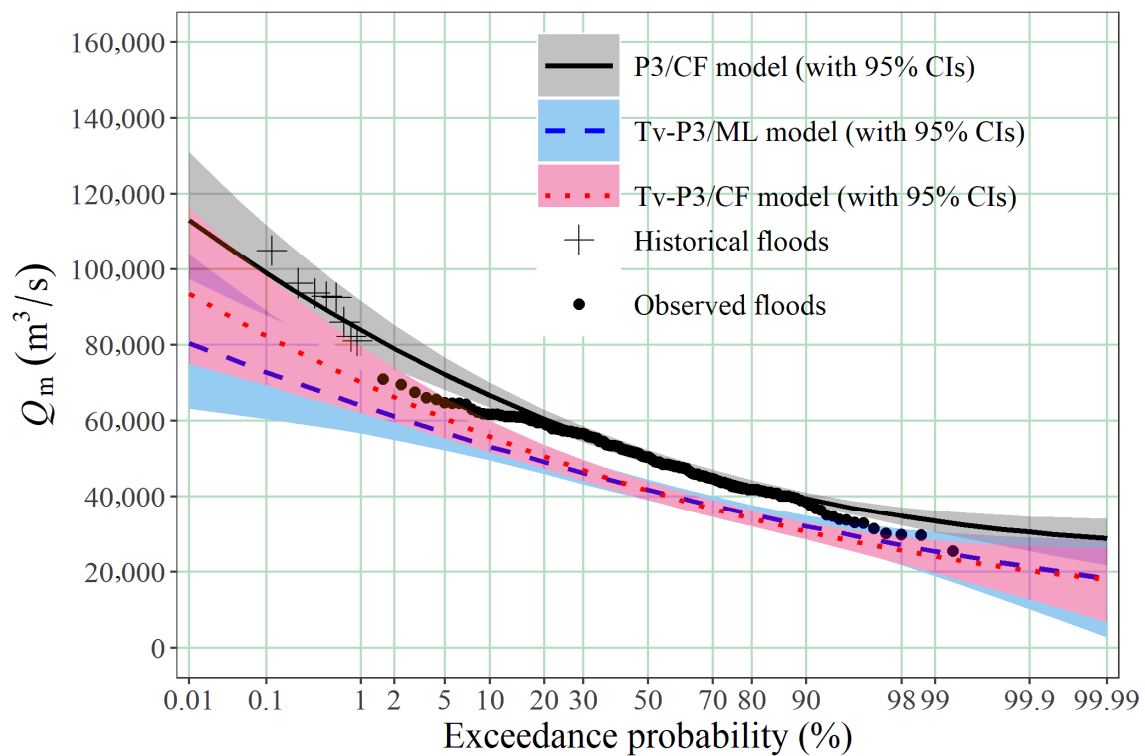

Figure 7. Comparison of P-III distribution frequency curves for flood peak Q_m under both stationary and non-stationary conditions (with MRI = 0.01843).

Table 5. Comparison of design flood estimation results for the TGR (flood peak: m^3/s, flood volume: 10^8 m^3).

Method/Model	Flood Variable	Parameter			Design Value					
		Mean	C_v	C_s	0.01%	0.10%	1%	2%	5%	10%
Stationary flood frequency analysis (P3/CF model)	Q_m	52,000	0.21	0.84	113,000	98,800	83,900	78,800	72,300	66,500
	W_{3d}	130	0.21	0.84	282.1	247	209.3	197.5	180.7	166.5
	W_{7d}	275	0.19	0.665	547.2	486.8	420.8	399.9	368.5	344.6
	W_{15d}	524	0.19	0.57	1022	911.8	796.5	757.5	702.2	656.1
	W_{30d}	935	0.18	0.54	1767	1590	1393	1327	1234	1158
Non-stationary flood frequency analysis (Tv-P3/ML model)	Q_m	42,700	0.195	0.396	80,900	73,200	64,400	61,500	57,200	53,600
					−28.41%	−25.91%	−23.24%	−21.95%	−20.89%	−19.40%
	W_{3d}	111.1	0.199	0.500	217.4	195.1	170.3	162.0	150.2	140.3
					−22.94%	−21.01%	−18.63%	−17.97%	−16.88%	−15.74%
	W_{7d}	234.0	0.190	0.394	438.0	396.8	350.2	334.5	311.9	292.6
					−19.96%	−18.49%	−16.78%	−16.35%	−15.36%	−15.09%
	W_{15d}	452.5	0.183	0.394	831.1	754.6	668.2	639.1	597.0	561.3
					−18.68%	−17.24%	−16.11%	−15.63%	−14.98%	−14.45%
	W_{30d}	822.9	0.178	0.388	1491	1356	1204	1153	1078	1015
					−15.62%	−14.72%	−13.57%	−13.11%	−12.64%	−12.35%
Non-stationary flood frequency analysis (Tv-P3/CF model)	Q_m	41,100	0.223	0.751	90,400	79,300	67,200	63,300	57,800	53,300
					−20.00%	−19.74%	−19.90%	−19.67%	−20.06%	−19.85%
	W_{3d}	98.1	0.230	0.808	222.4	193.9	163.3	153.4	139.5	128.2
					−21.16%	−21.50%	−21.98%	−22.33%	−22.80%	−23.00%
	W_{7d}	206.8	0.218	0.605	435.2	385.7	331.3	313.4	288.0	266.8
					−20.47%	−20.77%	−21.27%	−21.63%	−21.85%	−22.58%
	W_{15d}	433.3	0.191	0.616	854.3	762.8	662.4	629.3	582.4	543.4
					−16.41%	−16.34%	−16.84%	−16.92%	−17.06%	−17.18%
	W_{30d}	792.0	0.181	0.566	1503	1351	1183	1127	1048	982
					−14.94%	−15.03%	−15.08%	−15.07%	−15.07%	−15.20%

Taking the series of annual maximum design flood peak Q_m as an example, Figure 7 presents the P-III distribution frequency curves derived from the stationary P3/CF model and the non-stationary Tv-P3/ML and Tv-P3/CF models, respectively, all plotted on a Hessian probability graph [3]. It is important to note that the black data points in Figure 7 refer to empirical data that meet the stationary assumption and are used solely to illustrate the fitness of the P3/CF model. However, since the parameters of the P-III frequency curve under the non-stationary assumption varied with the MRI series, it was not possible to plot the corresponding empirical data points for the theoretical frequency curve. Therefore, Figure 7 only displays the time-varying P-III frequency curve after the operation of the key cascade reservoirs upstream of the TGR (i.e., MRI = 0.01843). Figure 7 shows: (a) The non-stationary time-varying P-III frequency curves lay below the stationary P3/CF results, further highlighting the significant reduction effect of upstream reservoir regulation on design floods. (b) The right tail of the curve derived from the Tv-P3/ML model was relatively flat, suggesting that it did not adequately account for the historical information in design flood estimation. (c) The TV-P3/CF model could be coupled with specific covariates (MRI) to forecast design floods in subsequent years in the event of the construction of new large reservoirs upstream of the study section in the future. Furthermore, the 95%

confidence intervals (CIs) of the models were computed using the bootstrap method [83]. The width of the CIs indicated that the stationary P3/CF model exhibited the smallest uncertainty, followed by the Tv-P3/CF model, while the Tv-P3/ML model had the largest uncertainty. Moreover, the Tv-P3/CF model could be used to estimate future design floods in the reservoir operation period by incorporating projected values of the modified reservoir index (MRI) for upcoming years. This approach allows for the calculation of design floods in scenarios involving the construction of new large reservoirs upstream. Furthermore, based on design floods in the reservoir operation period, the reservoir operation water level can be adjusted for management practices.

Severe floods occurred in both the main stream and main tributaries of the upper Yangtze River during the 1954 flood season [84]. Consequently, the 1954 flood hydrograph was selected as the typical flood hydrograph in this study. Using the peak and volume amplitude method, the flood variables obtained from the Tv-P3/CF model were amplified to derive the 1000-year return period design flood hydrograph in the reservoir operation period. The results, juxtaposed with the initial design flood hydrograph, are presented in Figure 8, which clearly demonstrates a significant reduction in the TGR's design flood hydrograph due to the regulation effects of the upstream cascade reservoirs. According to the reservoir operation rules, the flood control water level (FCWL) in the operation period is 154 m, which is higher than the flood-limited water level (FLWL) of 145 m in the construction period. Subsequently, we used the 1877–2022 daily flow discharge data from June to September to evaluate the reservoir operation risk and benefits of applying FCWL (FLWL). The results showed that the TGR could produce 5.02 (4.70) billion kW·h of hydropower in the operation (construction) period from June to September, increasing by 0.32 billion kW·h (+6.8%), and the flood prevention standards for the Jing River reach and Chenglingji section remained unchanged.
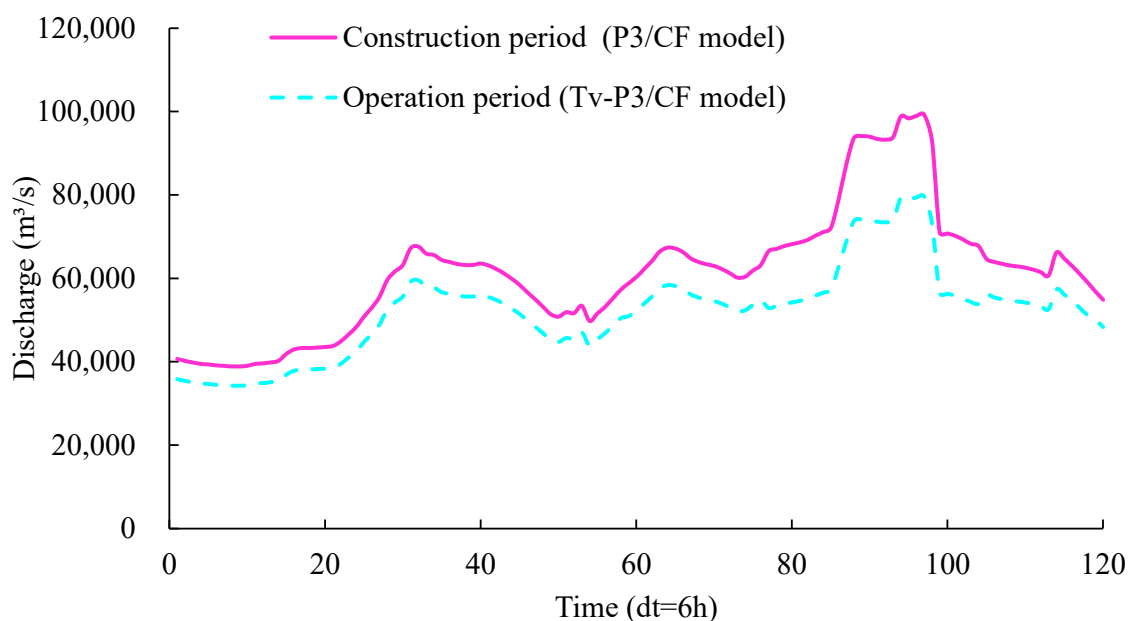

Figure 8. Comparison of the 1000-year design flood hydrographs in the construction and operation periods.

5. Discussion

Non-stationary flood frequency analysis applies a distribution function directly to the measured non-stationarity flood series, thus obviating the restoration of the observed flow series. However, this approach can only assess the effects of reservoirs on the flood series by integrating certain metrics that measure these impacts [85]. It does not explicitly incorporate the specific factors essential to reservoir operation, such as operation strategies,

characteristic parameters, and rule curves [86–88]. Therefore, this process is referred to as an "**implicit**" consideration of the reservoir's regulation influence. By contrast, the flood regional composition method employs the restored, stationary series of annual maximum floods and design flood hydrographs at the dam site for calculations. After analyzing the flood generation mechanism of the investigated reservoir, the design flood hydrograph is amplified according to the flood volumes in each sub-region and then progressively routed from upstream to downstream [8,21,89]. This approach strictly incorporates specific factors required in reservoir operation, thus providing an "**explicit**" consideration of the reservoir's regulation effects.

Both non-stationary flood frequency analysis and flood regional composition method indicated a reduction in the design flood hydrograph for downstream reservoirs, attributable to the regulation influence of upstream cascade reservoirs in the operation period. This reduction arose because the flood prevention storage of upstream reservoirs impounds a portion of the flood volume, thereby taking on part of the flood mitigation responsibilities [78]. This fundamental concept was explicitly represented in the flood regional composition method while the inherent structural limitations prevented this principle from being directly represented in the non-stationary flood frequency analysis. Although the non-stationary approach simplifies the calculations, it may lead to results that contradict the physical reality—such as a reduction in the design flood hydrograph that exceeds the collective flood prevention storage of the upstream reservoirs. Therefore, it is crucial to impose constraints to ensure that the outcomes remain consistent with the underlying hydrological processes.

6. Conclusions

This study presented a novel approach for non-stationary flood frequency analysis by incorporating historical information. Based on the monotonically increasing property of the distribution function of the continuous flood variables, a novel Tv-P3/CF model was proposed and compared with the Tv-P3/ML model. The non-stationary design floods in the TGR operation period were estimated and discussed. The main findings revealed:

(a) Both the reservoir index (RI) and modified reservoir index (MRI) can effectively capture the non-stationarity of the flood series, functioning as a covariate of the time-varying P-III distribution. The MRI provides a better fit for the flood series than the RI, with a small Akaike information criterion (AIC) value.

(b) The Q–Q plot-based curve fitting method produces a lower AIC value than the maximum likelihood method. The performance of the Tv-P3/CF model is superior to that of the Tv-P3/ML model, particular in fitting historical flood events.

(c) Compared to the original design floods of the TGR in the construction period, the non-stationary design flood peak and the 3-day and 7-day flood volumes are reduced by approximately 20%, while the 15-day and 30-day flood volumes are reduced by around 16%.

(d) The FLWL in the TGR operation period can be raised from 145 m to 154 m compared with the design value in the construction period. The economic benefits obtained from the new FLWL scheme are 0.32 billion kW·h (or increase by 6.8%) annually during flood season without increasing the flood prevention risks.

This study demonstrates that incorporating historical flood events can enhance the robustness of design flood estimation, especially in capturing the tail behavior of extreme flood events. The comparison with traditional stationary flood frequency methods underscores the necessity of adaptive management strategies that align with evolving hydrological conditions. We recommend further research to integrate non-stationary flood frequency results with reservoir management systems for decision making.

Author Contributions: Y.X.: Writing—original draft, Writing—review & editing, Visualization, Methodology, Formal analysis, Data curation, Conceptualization; S.G.: Writing—Review & editing, Project administration, Funding acquisition, Conceptualization; S.Z.: Conceptualization, Data curation; X.W.: Data curation, Calculation; J.T. and Z.L.: Data curation, Calculation. All authors have read and agreed to the published version of the manuscript.

References

1. Schendel, T.; Thongwichian, R. Considering Historical Flood Events in Flood Frequency Analysis: Is It Worth the Effort? *Adv. Water Resour.* **2017**, *105*, 144–153. [CrossRef]
2. MWR. *Specification for Calculating Design Flood of Water Resources and Hydropower Projects*; China Water & Power Press: Beijing, China, 2006. (In Chinese)
3. Yin, J.; Guo, S.; Liu, Z.; Yang, G.; Zhong, Y.; Liu, D. Uncertainty Analysis of Bivariate Design Flood Estimation and Its Impacts on Reservoir Routing. *Water Resour. Manag.* **2018**, *32*, 1795–1809. [CrossRef]
4. Zhong, Y.; Guo, S.; Liu, Z.; Wang, Y.; Yin, J. Quantifying Differences between Reservoir Inflows and Dam Site Floods Using Frequency and Risk Analysis Methods. *Stoch. Environ. Res. Risk Assess.* **2018**, *32*, 419–433. [CrossRef]
5. Li, X.; Guo, S.; Liu, P.; Chen, G. Dynamic Control of Flood Limited Water Level for Reservoir Operation by Considering Inflow Uncertainty. *J. Hydrol.* **2010**, *391*, 124–132. [CrossRef]
6. Xie, Y.; Guo, S.; Zhong, S.; He, Z.; Liu, P.; Zhou, Y. Optimal Allocation of Flood Prevention Storage and Dynamic Operation of Water Levels to Increase Cascade Reservoir Hydropower Generation. *Renew. Energy* **2024**, *228*, 120676. [CrossRef]
7. Liang, Z.; Yang, J.; Hu, Y.; Wang, J.; Li, B.; Zhao, J. A Sample Reconstruction Method Based on a Modified Reservoir Index for Flood Frequency Analysis of Non-Stationary Hydrological Series. *Stoch. Environ. Res. Risk Assess.* **2018**, *32*, 1561–1571. [CrossRef]
8. Xiong, F.; Guo, S.; Liu, P.; Xu, C.-Y.; Zhong, Y.; Yin, J.; He, S. A General Framework of Design Flood Estimation for Cascade Reservoirs in Operation Period. *J. Hydrol.* **2019**, *577*, 124003. [CrossRef]
9. Javelle, P.; Ouarda, T.B.M.J.; Lang, M.; Bobée, B.; Galéa, G.; Grésillon, J.-M. Development of Regional Flood-Duration–Frequency Curves Based on the Index-Flood Method. *J. Hydrol.* **2002**, *258*, 249–259. [CrossRef]
10. Milly, P.C.D.; Betancourt, J.; Falkenmark, M.; Hirsch, R.M.; Kundzewicz, Z.W.; Lettenmaier, D.P.; Stouffer, R.J. Stationarity Is Dead: Whither Water Management? *Science* **2008**, *319*, 573–574. [CrossRef]
11. Brandimarte, L.; Di Baldassarre, G. Uncertainty in Design Flood Profiles Derived by Hydraulic Modelling. *Hydrol. Res.* **2012**, *43*, 753–761. [CrossRef]
12. Vidrio-Sahagún, C.T.; Ruschkowski, J.; He, J.; Pietroniro, A. A Practice-Oriented Framework for Stationary and Nonstationary Flood Frequency Analysis. *Environ. Model. Softw.* **2024**, *173*, 105940. [CrossRef]
13. Jia, Y.; Sasani, M. Nonstationary Coastal Flood Hazard Analysis. *Nat. Hazards* **2024**, *120*, 7015–7037. [CrossRef]
14. Gao, S.; Liu, P.; Pan, Z.; Ming, B.; Guo, S.; Cheng, L.; Wang, J. Incorporating Reservoir Impacts into Flood Frequency Distribution Functions. *J. Hydrol.* **2019**, *568*, 234–246. [CrossRef]
15. Mohammadi, P.; Ebrahimi, K.; Bazrafshan, J. Flood Frequency Analysis under Nonstationary Modeling in the Gorganrood River Basin, Iran. *J. Hydrol. Eng.* **2023**, *28*, 05023004. [CrossRef]
16. Zeng, S.; Xia, J.; Du, H. Separating the Effects of Climate Change and Human Activities on Runoff over Different Time Scales in the Zhang River Basin. *Stoch. Environ. Res. Risk Assess.* **2014**, *28*, 401–413. [CrossRef]
17. Di Baldassarre, G.; Martinez, F.; Kalantari, Z.; Viglione, A. Drought and Flood in the Anthropocene: Feedback Mechanisms in Reservoir Operation. *Earth Syst. Dyn.* **2017**, *8*, 225–233. [CrossRef]
18. Shao, Y.; He, Y.; Mu, X.; Zhao, G.; Gao, P.; Sun, W. Contributions of Climate Change and Human Activities to Runoff and Sediment Discharge Reductions in the Jialing River, a Main Tributary of the Upper Yangtze River, China. *Theor. Appl. Climatol.* **2021**, *145*, 1437–1450. [CrossRef]
19. Xie, Y.; Guo, S.; Xiong, L.; Tian, J.; Xiong, F. Nonstationary Design Flood Estimation in Response to Climate Change, Population Growth and Cascade Reservoir Regulation. *Water* **2021**, *13*, 2687. [CrossRef]
20. Wang, M.; Jiang, S.; Ren, L.; Xu, C.-Y.; Shi, P.; Yuan, S.; Liu, Y.; Fang, X. Nonstationary Flood and Low Flow Frequency Analysis in the Upper Reaches of Huaihe River Basin, China, Using Climatic Variables and Reservoir Index as Covariates. *J. Hydrol.* **2022**, *612*, 128266. [CrossRef]
21. Guo, S.; Muhammad, R.; Liu, Z.; Xiong, F.; Yin, J. Design Flood Estimation Methods for Cascade Reservoirs Based on Copulas. *Water* **2018**, *10*, 560. [CrossRef]
22. Xiong, F.; Guo, S.; Yin, J.; Tian, J.; Rizwan, M. Comparative Study of Flood Regional Composition Methods for Design Flood Estimation in Cascade Reservoir System. *J. Hydrol.* **2020**, *590*, 125530. [CrossRef]
23. Zhang, Q.; Gu, X.; Singh, V.P.; Xiao, M.; Chen, X. Evaluation of Flood Frequency under Non-Stationarity Resulting from Climate Indices and Reservoir Indices in the East River Basin, China. *J. Hydrol.* **2015**, *527*, 565–575. [CrossRef]

24. Zhao, G.; Gao, H.; Naz, B.S.; Kao, S.-C.; Voisin, N. Integrating a Reservoir Regulation Scheme into a Spatially Distributed Hydrological Model. *Adv. Water Resour.* **2016**, *98*, 16–31. [CrossRef]

25. Zhao, G.; Bates, P.; Neal, J. The Impact of Dams on Design Floods in the Conterminous Us. *Water Resour. Res.* **2020**, *56*, e2019WR025380. [CrossRef]

26. Cipollini, S.; Fiori, A.; Volpi, E. A New Physically Based Index to Quantify the Impact of Multiple Reservoirs on Flood Frequency at the Catchment Scale Based on the Concept of Equivalent Reservoir. *Water Resour. Res.* **2022**, *58*, e2021WR031470. [CrossRef]

27. Li, S.; Qin, Y.; Liu, Y.; Song, X.; Liu, Q.; Li, Z. Estimating the Design Flood under the Influence of Check Dams by Removing Nonstationarity from the Flood Peak Discharge Series. *Hydrol. Res.* **2020**, *51*, 1261–1273. [CrossRef]

28. Li, S.; Qin, Y.; Song, X.; Bai, S.; Liu, Y. Nonstationary Frequency Analysis of the Weihe River Annual Runoff Series Using De-Nonstationarity Method. *J. Hydrol. Eng.* **2021**, *26*, 04021034. [CrossRef]

29. Yan, L.; Xiong, L.; Ruan, G.; Xu, C.-Y.; Yan, P.; Liu, P. Reducing Uncertainty of Design Floods of Two-Component Mixture Distributions by Utilizing Flood Timescale to Classify Flood Types in Seasonally Snow Covered Region. *J. Hydrol.* **2019**, *574*, 588–608. [CrossRef]

30. He, C.; Chen, F.; Wang, Y.; Long, A.; He, X. Flood Frequency Analysis of Manas River Basin in China under Non-Stationary Condition. *J. Flood Risk Manag.* **2021**, *14*, e12745. [CrossRef]

31. Zhang, H.; Dou, Y.; Ye, L.; Zhang, C.; Yao, H.; Bao, Z.; Tang, Z.; Wang, Y.; Huang, Y.; Zhu, S.; et al. Realizing the Full Reservoir Operation Potential during the 2020 Yangtze River Floods. *Sci. Rep.* **2022**, *12*, 2822. [CrossRef]

32. Strupczewski, W.G.; Singh, V.P.; Feluch, W. Non-Stationary Approach to at-Site Flood Frequency Modelling I. Maximum Likelihood Estimation. *J. Hydrol.* **2001**, *248*, 123–142. [CrossRef]

33. Strupczewski, W.G.; Singh, V.P.; Mitosek, H.T. Non-Stationary Approach to at-Site Flood Frequency Modelling. III. Flood Analysis of Polish Rivers. *J. Hydrol.* **2001**, *248*, 152–167. [CrossRef]

34. Strupczewski, W.G.; Kaczmarek, Z. Non-Stationary Approach to at-Site Flood Frequency Modelling II. Weighted Least Squares Estimation. *J. Hydrol.* **2001**, *248*, 143–151. [CrossRef]

35. Rigby, R.A.; Stasinopoulos, D.M. Generalized Additive Models for Location, Scale and Shape. *J. R. Stat. Soc. Ser. C Appl. Stat.* **2005**, *54*, 507–554. [CrossRef]

36. Stasinopoulos, D.M.; Rigby, R.A. Generalized Additive Models for Location Scale and Shape (GAMLSS) in R. *J. Stat. Softw.* **2007**, *23*, 1–46. [CrossRef]

37. Xiong, B.; Xiong, L.; Guo, S.; Xu, C.-Y.; Xia, J.; Zhong, Y.; Yang, H. Nonstationary Frequency Analysis of Censored Data: A Case Study of the Floods in the Yangtze River from 1470 to 2017. *Water Resour. Res.* **2020**, *56*, e2020WR027112. [CrossRef]

38. Wang, L.; Guo, S.; Wang, J.; Chen, Y.; Qiu, H.; Zhang, J.; Wei, X. A Novel Multi-Scale Standardized Index Analyzing Monthly to Sub-Seasonal Drought-Flood Abrupt Alternation Events in the Yangtze River Basin. *J. Hydrol.* **2024**, *633*, 130999. [CrossRef]

39. Faulkner, D.S.; Longfield, S.; Warren, S.; Tawn, J.A. Modelling Non-Stationary Flood Frequency in England and Wales Using Physical Covariates. *Hydrol. Res.* **2024**, *55*, 205–220. [CrossRef]

40. López, J.; Francés, F. Non-Stationary Flood Frequency Analysis in Continental Spanish Rivers, Using Climate and Reservoir Indices as External Covariates. *Hydrol. Earth Syst. Sci.* **2013**, *17*, 3189–3203. [CrossRef]

41. Li, R.; Xiong, L.; Zha, X.; Xiong, B.; Liu, H.; Chen, J.; Zeng, L.; Li, W. Impacts of Climate and Reservoirs on the Downstream Design Flood Hydrograph: A Case Study of Yichang Station. *Nat. Hazards* **2022**, *113*, 1803–1831. [CrossRef]

42. Zhang, T.; Su, X.; Feng, K. The Development of a Novel Nonstationary Meteorological and Hydrological Drought Index Using the Climatic and Anthropogenic Indices as Covariates. *Sci. Total Environ.* **2021**, *786*, 147385. [CrossRef]

43. Guo, S.; Xiong, L.; Chen, J.; Guo, S.; Xia, J.; Zeng, L.; Xu, C.-Y. Nonstationary Regional Flood Frequency Analysis Based on the Bayesian Method. *Water Resour. Manag.* **2023**, *37*, 659–681. [CrossRef]

44. Brodeur, Z.; Wi, S.; Shabestanipour, G.; Lamontagne, J.; Steinschneider, S. A Hybrid, Non-Stationary Stochastic Watershed Model (Swm) for Uncertain Hydrologic Simulations under Climate Change. *Water Resour. Res.* **2024**, *60*, e2023WR035042. [CrossRef]

45. Anzolin, G.; De Oliveira, D.Y.; Vrugt, J.A.; AghaKouchak, A.; Chaffe, P.L.B. Nonstationary Frequency Analysis of Extreme Precipitation: Embracing Trends in Observations. *J. Hydrol.* **2024**, *637*, 131300. [CrossRef]

46. Koutrouvelis, I.A.; Canavos, G.C. Estimation in the Pearson Type 3 Distribution. *Water Resour. Res.* **1999**, *35*, 2693–2704. [CrossRef]

47. Hosking, J.R.M.; Wallis, J.R. The Value of Historical Data in Flood Frequency Analysis. *Water Resour. Res.* **1986**, *22*, 1606–1612. [CrossRef]

48. Guo, S. Nonparametric Variable Kernel Estimation with Historical Floods and Paleoflood Information. *Water Resour. Res.* **1991**, *27*, 91–98. [CrossRef]

49. Payrastre, O.; Gaume, E.; Andrieu, H. Usefulness of Historical Information for Flood Frequency Analyses: Developments Based on a Case Study. *Water Resour. Res.* **2011**, *47*, W08511. [CrossRef]

50. Mann, H.B. Nonparametric Tests against Trend. *Econometrica* **1945**, *13*, 245–259. [CrossRef]

51. Kendall, M.G. *Rank Correlation Methods*; Rank Correlation Methods; Griffin: Oxford, UK, 1948.

52. Yue, S.; Pilon, P.; Cavadias, G. Power of the Mann–Kendall and Spearman's Rho Tests for Detecting Monotonic Trends in Hydrological Series. *J. Hydrol.* **2002**, *259*, 254–271. [CrossRef]

53. Pettitt, A.N. A Non-Parametric Approach to the Change-Point Problem. *J. R. Stat. Soc. Ser. C Appl. Stat.* **1979**, *28*, 126–135. [CrossRef]

54. Liu, D.; Guo, S.; Lian, Y.; Xiong, L.; Chen, X. Climate-Informed Low-Flow Frequency Analysis Using Nonstationary Modelling. *Hydrol. Process.* **2015**, *29*, 2112–2124. [CrossRef]

55. Yin, J.; Guo, S.; Liu, Z.; Chen, K.; Chang, F.-J.; Xiong, F. Bivariate Seasonal Design Flood Estimation Based on Copulas. *J. Hydrol. Eng.* **2017**, *22*, 05017028. [CrossRef]

56. Li, N.; Guo, S.; Xiong, F.; Wang, J.; Xie, Y. Comparative Study of Flood Coincidence Risk Estimation Methods in the Mainstream and Its Tributaries. *Water Resour. Manag.* **2022**, *36*, 683–698. [CrossRef]

57. Li, H.; Liu, P.; Guo, S.; Cheng, L.; Yin, J. Climatic Control of Upper Yangtze River Flood Hazard Diminished by Reservoir Groups. *Environ. Res. Lett.* **2020**, *15*, 124013. [CrossRef]

58. Guo, S.; Cunnane, C. Evaluation of the Usefulness of Historical and Palaeological Floods in Quantile Estimation. *J. Hydrol.* **1991**, *129*, 245–262. [CrossRef]

59. Li, T.; Guo, S.; Chen, L.; Guo, J. Bivariate Flood Frequency Analysis with Historical Information Based on Copula. *J. Hydrol. Eng.* **2013**, *18*, 1018–1030. [CrossRef]

60. Xiong, L.; Jiang, C.; Guo, S.; Li, S.; Li, R.; Li, W. Multivariate Dam-Site Flood Frequency Analysis of the Three Gorges Reservoir Considering Future Reservoir Regulation and Precipitation. *Water* **2022**, *14*, 138. [CrossRef]

61. Batalla, R.J.; Gómez, C.M.; Kondolf, G.M. Reservoir-Induced Hydrological Changes in the Ebro River Basin (NE Spain). *J. Hydrol.* **2004**, *290*, 117–136. [CrossRef]

62. Xiong, B.; Xiong, L.; Xia, J.; Xu, C.-Y.; Jiang, C.; Du, T. Assessing the Impacts of Reservoirs on Downstream Flood Frequency by Coupling the Effect of Scheduling-Related Multivariate Rainfall with an Indicator of Reservoir Effects. *Hydrol. Earth Syst. Sci.* **2019**, *23*, 4453–4470. [CrossRef]

63. Cui, H.; Jiang, S.; Gao, B.; Ren, L.; Xiao, W.; Wang, M.; Ren, M.; Xu, C.-Y. On Method of Regional Non-Stationary Flood Frequency Analysis under the Influence of Large Reservoir Group and Climate Change. *J. Hydrol.* **2023**, *618*, 129255. [CrossRef]

64. Katz, R.W.; Parlange, M.B.; Naveau, P. Statistics of Extremes in Hydrology. *Adv. Water Resour.* **2002**, *25*, 1287–1304. [CrossRef]

65. Du, T.; Xiong, L.; Xu, C.-Y.; Gippel, C.J.; Guo, S.; Liu, P. Return Period and Risk Analysis of Nonstationary Low-Flow Series under Climate Change. *J. Hydrol.* **2015**, *527*, 234–250. [CrossRef]

66. Jiang, C.; Xiong, L.; Xu, C.-Y.; Yan, L. A River Network-Based Hierarchical Model for Deriving Flood Frequency Distributions and Its Application to the Upper Yangtze Basin. *Water Resour. Res.* **2021**, *57*, e2020WR029374. [CrossRef]

67. Zhong, S.; Guo, S.; Wang, Y.; Wang, H.; Xie, Y.; Xu, C. A Novel Joint Probability Density Difference Approach for Assessing the Alteration of Hydrologic Regime. *River Res. Appl.* **2024**, *40*, 659–672. [CrossRef]

68. Hirose, H. Maximum Likelihood Parameter Estimation in the Three-Parameter Gamma Distribution. *Comput. Stat. Data Anal.* **1995**, *20*, 343–354. [CrossRef]

69. Wilk, M.B.; Gnanadesikan, R. Probability Plotting Methods for the Analysis of Data. *Biometrika* **1968**, *55*, 1–17. [CrossRef]

70. Stanford, J.L.; Vardeman, S.B. *Statistical Methods for Physical Science*; Academic Press: Cambridge, UK, 1994; ISBN 978-0-08-086016-9.

71. Zhang, L.; Singh, V.P. Revisiting the Application of Halphen Distributions in Flood Frequency Analysis. *J. Hydrol. Eng.* **2021**, *26*, 04021042. [CrossRef]

72. Akaike, H. A New Look at the Statistical Model Identification. *IEEE Trans. Autom. Control* **1974**, *19*, 716–723. [CrossRef]

73. Cole, T.J.; Green, P.J. Smoothing Reference Centile Curves: The LMS Method and Penalized Likelihood. *Stat. Med.* **1992**, *11*, 1305–1319. [CrossRef]

74. Xiao, Y.; Guo, S.; Liu, P.; Yan, B.; Chen, L. Design Flood Hydrograph Based on Multicharacteristic Synthesis Index Method. *J. Hydrol. Eng.* **2009**, *14*, 1359–1364. [CrossRef]

75. Zhou, Y.; Guo, S.; Xu, C.-Y.; Liu, P.; Qin, H. Deriving Joint Optimal Refill Rules for Cascade Reservoirs with Multi-Objective Evaluation. *J. Hydrol.* **2015**, *524*, 166–181. [CrossRef]

76. Yang, G.; Guo, S.; Liu, P.; Li, L.; Xu, C. Multiobjective Reservoir Operating Rules Based on Cascade Reservoir Input Variable Selection Method. *Water Resour. Res.* **2017**, *53*, 3446–3463. [CrossRef]

77. Yang, G.; Guo, S.; Liu, P.; Block, P. Sensitivity of Forecast Value in Multiobjective Reservoir Operation to Forecast Lead Time and Reservoir Characteristics. *J. Water Resour. Plan. Manag.* **2021**, *147*, 04021027. [CrossRef]

78. Xiong, F.; Xie, Y.; Guo, S.; Li, Y.; Yin, J.; Li, N. Equivalent Relationship between Flood Prevention Storage of Cascade Reservoirs in the Downstream Jinsha River and Three Gorges Reservoir. *J. Water Resour. Plan. Manag.* **2023**, *149*, 05023005. [CrossRef]

79. YWRC. *Hydrologic Inscription Cultural Relics in the Three Gorges Reservoir*; Science Press: Beijing, China, 1996.

80. Shu, W.; Li, Q.; Bao, Z.; Zhang, Y. Study on the Relationship between Reservoir Inflow Flood and Dam Site Flood in Three Gorges Reservoir. *Water Power* **2017**, *43*, 10–14. [CrossRef]

81. Chen, M. Characteristics and Enlightenment of Rainstorm and Flood in Yangtze River in 2020. *Yangtze River* **2020**, *51*, 76–81. (In Chinese) [CrossRef]

82. Huang, Y. Practice and reflections on joint operation scheme of water projects of Changjiang River Basin: Flood control and water projects operation in 2020 flood. *Yangtze River* **2020**, *51*, 116–128+134. [CrossRef]

83. Ouarda, T.B.M.J.; Charron, C.; St-Hilaire, A. Uncertainty of Stationary and Nonstationary Models for Rainfall Frequency Analysis. *Int. J. Climatol.* **2020**, *40*, 2373–2392. [CrossRef]

84. Yin, H.; Li, C. Human Impact on Floods and Flood Disasters on the Yangtze River. *Geomorphology* **2001**, *41*, 105–109. [CrossRef]

85. Yılmaz, M.; Tosunoğlu, F. Non-Stationary Low Flow Frequency Analysis under Climate Change. *Theor. Appl. Climatol.* **2024**, *155*, 7479–7497. [CrossRef]

86. Yang, G.; Zaitchik, B.; Badr, H.; Block, P. A Bayesian Adaptive Reservoir Operation Framework Incorporating Streamflow Non-Stationarity. *J. Hydrol.* **2021**, *594*, 125959. [CrossRef]

87. He, S.; Guo, S.; Zhang, J.; Liu, Z.; Cui, Z.; Zhang, Y.; Zheng, Y. Multi-Objective Operation of Cascade Reservoirs Based on Short-Term Ensemble Streamflow Prediction. *J. Hydrol.* **2022**, *610*, 127936. [CrossRef]

88. Yang, G.; Giuliani, M.; Galelli, S. Valuing the Codesign of Streamflow Forecast and Reservoir Operation Models. *J. Water Resour. Plan. Manag.* **2023**, *149*, 04023037. [CrossRef]

89. Zhong, S.; Guo, S.; He, Y.; Xie, Y. A Novel Flood Regional Composition Method for Design Flood Estimation in the Cascade Reservoirs. *Water* **2024**, *16*, 2190. [CrossRef]